

AperTO - Archivio Istituzionale Open Access dell'Università di Torino

**P-T evolution of elusive UHP eclogites from the Luotian dome (north Dabie zone, China): how far can the thermodynamic modeling lead us?**

**This is the author's manuscript**

*Original Citation:*

*Availability:*

This version is available <http://hdl.handle.net/2318/1507477> since 2017-05-17T23:13:01Z

*Published version:*

DOI:10.1016/j.lithos.2014.11.013

*Terms of use:*

Open Access

Anyone can freely access the full text of works made available as "Open Access". Works made available under a Creative Commons license can be used according to the terms and conditions of said license. Use of all other works requires consent of the right holder (author or publisher) if not exempted from copyright protection by the applicable law.


(Article begins on next page)

Dear Author,

Please, note that changes made to the HTML content will be added to the article before publication, but are not reflected in this PDF.

Note also that this file should not be used for submitting corrections.

## AUTHOR QUERY FORM

 ELSEVIER	<b>Journal: LITHOS</b>  <b>Article Number: 3446</b>	<b>Please e-mail or fax your responses and any corrections to:</b> <b>Shivaram, Rohini</b> <b>E-mail: <a href="mailto:Corrections.ESCH@elsevier.spitech.com">Corrections.ESCH@elsevier.spitech.com</a></b> <b>Fax: +1 619 699 6721</b>
---	---	---

Dear Author,

Please check your proof carefully and mark all corrections at the appropriate place in the proof (e.g., by using on-screen annotation in the PDF file) or compile them in a separate list. Note: if you opt to annotate the file with software other than Adobe Reader then please also highlight the appropriate place in the PDF file. To ensure fast publication of your paper please return your corrections within 48 hours.

For correction or revision of any artwork, please consult <http://www.elsevier.com/artworkinstructions>.

We were unable to process your file(s) fully electronically and have proceeded by

☐ Scanning (parts of) your article

☐ Rekeying (parts of) your article

☐ Scanning the artwork

Any queries or remarks that have arisen during the processing of your manuscript are listed below and highlighted by flags in the proof. Click on the 'Q' link to go to the location in the proof.

Location in article	<b>Query / Remark: <a href="#">click on the Q link to go</a></b> <b>Please insert your reply or correction at the corresponding line in the proof</b>
<a href="#"><u>Q1</u></a>	The citation "Morimoto et al., 1988" has been changed to match the author name/date in the reference list. Please check here and in subsequent occurrences, and correct if necessary.
<a href="#"><u>Q2</u></a>	The citation "Langone et al., 2010" has been changed to match the author name/date in the reference list. Please check here and in subsequent occurrences, and correct if necessary.
<a href="#"><u>Q3</u></a>	Uncited reference: This section comprises references that occur in the reference list but not in the body of the text. Please position each reference in the text or, alternatively, delete it. Thank you.
<a href="#"><u>Q4</u></a>	Supplementary caption was not provided. Please check suggested data if appropriate and correct if necessary.
<a href="#"><u>Q5</u></a>	Please provide an update for reference "Liu et al., in press".
<a href="#"><u>Q6</u></a>	Please confirm that given names and surnames have been identified correctly.  <div data-bbox="638 1549 1133 1665" style="border: 1px solid black; padding: 10px; display: inline-block;">             Please check this box if you have no corrections to make to the PDF file. <input type="checkbox"/> </div>

Thank you for your assistance.



Contents lists available at ScienceDirect

Lithos

journal homepage: [www.elsevier.com/locate/lithos](http://www.elsevier.com/locate/lithos)

## Highlights

**P-T evolution of elusive UHP eclogites from the Luotian dome (North Dabie Zone, China): How far can the thermodynamic modeling lead us?**

Lithos xxx (2014) xxx – xxx

Chiara Groppo <sup>a,\*</sup>, Franco Rolfo <sup>a,b</sup>, Yi-Can Liu <sup>c</sup>, Liang-Peng Deng <sup>c</sup>, An-Dong Wang <sup>c</sup><sup>a</sup> Department of Earth Sciences, University of Torino, Torino, I 10125, Italy<sup>b</sup> IGG-CNR, Via Valperga Caluso 35, 10125 Turin, Italy<sup>c</sup> CAS Key Laboratory of Crust-Mantle Materials and Environments, School of Earth and Space Sciences, University of Science and Technology of China, 230026, Hefei, China

- The NDZ is characterized by widespread anatexis that overprinted the HP/UHP metamorphism.
- We present a petrologic study on two eclogites from the Luotian dome of the NDZ.
- Thermodynamic modelling allowed constraining the prograde P-T evolution of the NDZ.
- Unambiguous evidence of UHP conditions have not been found.
- Other more suitable methods can constrain UHP history in “really hot & slow” terranes.







Contents lists available at ScienceDirect

Lithos

journal homepage: [www.elsevier.com/locate/lithos](http://www.elsevier.com/locate/lithos)

# P-T evolution of elusive UHP eclogites from the Luotian dome (North Dabie Zone, China): How far can the thermodynamic modeling lead us?

Chiara Groppo<sup>a,\*</sup>, Franco Rolfo<sup>a,b</sup>, Yi-Can Liu<sup>c</sup>, Liang-Peng Deng<sup>c</sup>, An-Dong Wang<sup>c</sup>

<sup>a</sup> Department of Earth Sciences, University of Torino, Torino, I 10125, Italy

<sup>b</sup> IGG-CNR, Via Valperga Caluso 35, 10125 Turin, Italy

<sup>c</sup> CAS Key Laboratory of Crust-Mantle Materials and Environments, School of Earth and Space Sciences, University of Science and Technology of China, 230026, Hefei, China

## ARTICLE INFO

### Article history:

Received 19 March 2014

Accepted 15 November 2014

Available online xxxx

### Keywords:

Ultra-high pressure metamorphism

Granulitized eclogite

Thermodynamic modelling

P-T evolution

North Dabie Complex Zone

## ABSTRACT

In those ultrahigh pressure (UHP) terranes that experienced protracted high/ultrahigh temperature (HT/UHT) exhumation histories, slow exhumation rates and a widespread anatexis, the UHP metamorphism is often elusive and difficult to be constrained. In the Dabie-Sulu orogenic belt of central-eastern China, which is the largest UHP terrane in the world, the migmatitic North Dabie complex Zone (NDZ) stands out for the widespread anatexis that widely overprinted the traces of eclogite-facies metamorphism, hampering a precise reconstruction of its P-T(t) evolution.

Different peak P-T conditions, varying between non-eclogitic to UHP conditions, have been proposed so far for various high-grade metamorphic rocks from the NDZ. Few attempts were also made to reconstruct its P-T evolution. Most of the proposed P-T paths, based on conventional thermobarometry, follow a clockwise trajectory at relatively HT (> 750 °C) and almost none of them infer the prograde portion.

In this paper we present a detailed petrologic study on two eclogites from the Luotian dome of the NDZ: sample 11-7c2 shows a well preserved eclogitic assemblage (Grt + Cpx + Rt), whereas sample 11-9c1 is a Qtz-Ky-bearing eclogite pervasively retrogressed under granulite-facies conditions. The results of the thermodynamic forward modelling allowed to constrain, for the first time, the prograde portion of the NDZ P-T evolution; the decompression evolution at granulite-facies conditions has been also precisely constrained. However, due to the HT overprinting and to poorly reactive bulk compositions, this method alone is not sufficient to reconstruct the whole P-T trajectory of the NDZ: more specifically, unambiguous evidence of the attainment of UHP conditions have not been found. Different “unconventional” thermobarometric methods (such as those based on trace element and textural characterization of zircons) might be more suitable to decipher the HP/UHP history of this “really hot and slow” UHP terrane.

© 2014 Elsevier B.V. All rights reserved.

## 1. Introduction

The Dabie Shan metamorphic belt in central China, formed by continental collision between the South China Block and the North China Block in the Triassic (e.g. Zhang et al., 2009 and references therein), is the largest high-pressure/ultrahigh-pressure (HP/UHP) terrane in the world. While in the Central Dabie Zone the UHP metamorphism was discovered almost 25 years ago (Okay et al., 1989; Wang et al., 1989), in the North Dabie Zone (NDZ) UHP peak metamorphic conditions have been suggested only since about 10 years (e.g. Liu et al., 2007a,b, 2011a,b; Malaspina et al., 2006; Xu et al., 2003, 2005). This apparent discrepancy may be due to the fact that the NDZ experienced a protracted high-temperature/ultrahigh-temperature (HT/UHT) metamorphic evolution (e.g. Faure et al., 2003; Liu et al.,

2001, 2005, 2007a,b, 2011a,b; Xiao et al., 2001, 2005; Zhang et al., 1996) that widely overprinted the traces of eclogite-facies metamorphism.

Direct clues of UHP metamorphism in the NDZ are rare and have been a matter of discussion for a long time (see the (Tong et al., 2011; Zhang et al., 2009) reviews, and references therein). The most convincing UHP evidence are the few diamond inclusions discovered in zircons from both eclogites (Xu et al., 2003) and granitic gneisses (Liu et al., 2007b), and a relic coesite inclusion in zircon and quartz pseudomorphs after coesite enclosed in garnet from eclogites (Liu et al., 2011a); other features, such as exsolution-type microstructures in garnet and/or clinopyroxene, are more debated. Except for these few examples, UHP metamorphism in the NDZ remains quite elusive and difficult to be unambiguously demonstrated.

Different peak P-T conditions have been proposed for the NDZ since the last decade (see Tong et al., 2011 for a review), most of them based on conventional thermobarometry (e.g. Chen et al., 2006; Liu et al., 2007a; Malaspina et al., 2006; Tsai and Liou, 2000; Xiao et al., 2001, 2005). Estimates of the maximum pressures for various high-grade

\* Corresponding author at: Department of Earth Sciences, University of Torino, Via Vaperga Caluso, 35, Torino, I 10125, Italy. Tel.: +39 0116705106.  
E-mail address: [chiara.groppo@unito.it](mailto:chiara.groppo@unito.it) (C. Groppo).

metamorphic rocks from the NDZ vary between non-eclogitic conditions (Paleoproterozoic felsic granulites; Chen et al., 2006; Wu et al., 2008) to HP and UHP conditions (Triassic eclogites and granitic gneisses, > 40 kbar; e.g. Liu et al., 2007a,b, 2011a,b; Xu et al., 2005). Basing on conventional thermobarometry applied to different mineral assemblages, few attempts were also made to reconstruct the whole P-T evolution of the NDZ (e.g. Faure et al., 2003; Liu et al., 2011a; Xiao et al., 2001, 2005). Most of the proposed P-T paths follow a clockwise trajectory at relatively HT (> 750 °C) and almost none of them infer the prograde portion (i.e. the P-T evolution prior to the attainment of maximum peak-P). More recently, Liu et al. (in press) constrained the whole retrograde P-T-t evolution of the NDZ granulitized eclogites by combining the Zr-in-rutile and Ti-in-zircon thermometers with zircon U-Pb ages, and provided evidence of a multistage HT (and possibly UHT) evolution, from UHP eclogite-facies conditions to granulite-facies overprinting.

What is actually missing in this plethora of P-T(t) data is the contribution of the forward modelling approach to the reconstruction of the NDZ P-T evolution. Application of the phase petrology methods (e.g. P-T pseudosections) to eclogite-facies rocks pervasively overprinted by HT/UHT assemblages is particularly challenging. In fact, the widespread occurrence in these rocks of symplectitic and/or coronitic reaction textures, clearly suggests that equilibrium was attained only at a domainal scale. However, recent progresses have been made in the petrologic modelling of such complex rocks, demonstrating that it is actually possible to successfully apply phase petrology methods based on the principles of equilibrium thermodynamic also to texturally non-equilibrated rocks (e.g. Cruciani et al., 2008, 2011, 2012; Groppo et al., 2007a; Tajčmanová et al., 2006).

In this paper we present a detailed petrologic study on two granulitized eclogites from the Luotian dome of the NDZ. The aim of the study is twofold: (i) to constrain the whole P-T path of the eclogites using, for the first time, the pseudosection approach, particularly focusing on their prograde evolution which is totally unknown; (ii) to test the applicability of the thermodynamic forward modelling methods for deciphering the metamorphic history of such elusive UHP rocks. The results of this study allow to discuss and explain why evidence of UHP metamorphism are so rare in the NDZ, and suggest which methods might be useful in the future to more precisely constrain the maximum P and T experienced in the NDZ.

## 2. Geological setting

### 2.1. The North Dabie Zone

The Dabie orogen, located in the central portion of the Triassic Dabie-Sulu orogenic belt in central-eastern China, resulted from northward subduction of the South China Block beneath the North China Block (e.g. Ames et al., 1996; Bryant et al., 2004; Chavagnac and Jahn, 1996; Cong, 1996; Faure et al., 1999; Hacker et al., 2000; Li et al., 1993; Liou et al., 2009; Liu et al., 2005, 2006; Xu et al., 1992; Zhang et al., 2009). From north to south, the Dabie orogen is divided into five, fault-bounded, major lithotectonic units (e.g. Liu et al., 2007a; Tong et al., 2011; Xu et al., 2003; Zhang et al., 2009): (i) the low-grade Beihuaiyang Zone (BZ); (ii) the high-T migmatitic North Dabie complex Zone (NDZ); (iii) the Central Dabie UHP metamorphic Zone (CDZ); (iv) the South Dabie low-T eclogite Zone (SDZ); and (v) the Susong complex Zone (SZ) (Fig. 1a).

The NDZ mainly consists of tonalitic and granitic orthogneisses and post-collisional Cretaceous intrusions (Xie et al., 2006; Zhao et al., 2004, 2007) with subordinate meta-peridotite, garnet pyroxenite, garnet-bearing amphibolite, granulite and eclogite. Differently from the CDZ and the SDZ, in which the UHP/HP eclogite-facies stage was followed by cooling and decompression (e.g., Li et al., 2004; Rolfo et al., 2004; Xu et al., 1992), the NDZ experienced a pervasive granulite-facies overprinting accompanied by extensive partial melting

and migmatitization (e.g., Liu et al., 2001, 2005, 2007a,b, 2011a; Malaspina et al., 2006; Xiao et al., 2001; Xu et al., 2000) that partially or completely obliterated the evidence of the earlier metamorphic events at HP/UHP conditions. In spite of this pervasive HT overprinting, in the last ten years an increasing number of UHP/HP eclogite relics have been reported from the NDZ (e.g. Liu et al., 2005, 2007a; Tsai and Liou, 2000; Xu et al., 2003, 2005). Although the evidence of UHP metamorphism in the NDZ have been a matter of debate for many years (e.g. Ernst et al., 2007; Jahn and Chen, 2007; Zhang et al., 2009), the Triassic zircon U-Pb ages (220–240 Ma: Liu et al., 2000, 2007a, 2011b; Wang et al., 2012; Zhao et al., 2008) and Sm-Nd ages (Liu et al., 2005) of these eclogites suggest that these rocks formed by the Triassic subduction of the South China Block, similarly to those from the CDZ and SDZ. The Triassic metamorphic ages (Liu et al., 2000, 2007b; Xie et al., 2010) and the occurrence of micro-diamond inclusions in zircon and garnet (Liu et al., 2007b) from the NDZ migmatitic orthogneisses suggest that also the gneisses hosting the eclogites were involved in the Triassic deep subduction of the South China Block, thus implying that the NDZ experienced UHP metamorphism as a coherent unit.

The precise P-T-t evolution of the NDZ is still not well constrained and a multitude of P-T(t) paths have been proposed (Tong et al., 2011 and references therein). Most of the data point to a complex multistage evolution characterized by a nearly isothermal decompression at HT/UHT conditions. According to Liu et al. (2007a, 2011a) and Gu (2012), this HT/UHT evolution was associated to at least two stages of partial melting, i.e. decompression melting at  $207 \pm 4$  Ma and heating melting at  $\sim 130$  Ma during continental collision.

### 2.2. The Luotian dome granulitized eclogites

The Luotian dome in the south-western segment of the NDZ (Fig. 1a) is a deeply eroded area with both felsic and mafic granulites (Chen et al., 1998, 2006; Liu et al., 2007a; Wu et al., 2008). Eclogites occur as lenses or blocks, up to 3 m thick, in garnet-bearing migmatitic tonalitic gneisses (Liu et al., 2007a, 2011a,b). Due to the scarcity of outcrops, the direct contact between the eclogites and the hosting orthogneisses is rarely visible. Fresh eclogites are generally preserved in the core of these lenses, whereas they are retrogressed into garnet-bearing amphibolites towards the rim.

The studied samples were collected at Jinjiapu (sample 11-7c2) and Shiqiaopu (sample 11-9c1). At Jinjiapu (N30°54'14.8", E115°37'12.7"; 150 m a.s.l.), eclogites occur as metric lenses within migmatitic banded gneisses. Two domains are clearly visible in the eclogite at the outcrop scale: (i) fine-grained dark well-preserved eclogites with mm-sized red garnet and green omphacite are alternated to (ii) pale green domains mainly consisting of relatively coarse-grained clinopyroxene + plagioclase symplectites. Coarse-grained cm-sized rutile grains occur in both domains. Both domains are crosscut by a network of late mm-wide veins along which a pervasive amphibolization may be observed. Sample 11-7c2 (Fig. 1b) is representative of the well-preserved eclogite domain.

At Shiqiaopu (N30°47'17.5", E115°33'13.5"; 170 m a.s.l.), eclogites occur as smaller lenses and the relations with the hosting migmatitic gneisses were not observed. Two different types of eclogites were collected: (i) a pale-green, quartz-garnet-bearing strongly amphibolitized rock, characterized by mm-sized dark spots surrounded by a whitish corona, and (ii) a fine-grained dark-green eclogite with mm-sized garnet, crosscut by quartz + rutile veins. Sample 11-9c1 (Fig. 1b) is representative of the first rock type.

## 3. Petrography and mineral chemistry

The main microstructural features of samples 11-7c2 and 11-9c1 are shown in Figs. 2–3 and summarized in Fig. 4. Minerals were analysed with a Cambridge Stereoscan 360 SEM equipped with an EDS Energy 200 and a Pentafet detector (Oxford Instruments) at the Department



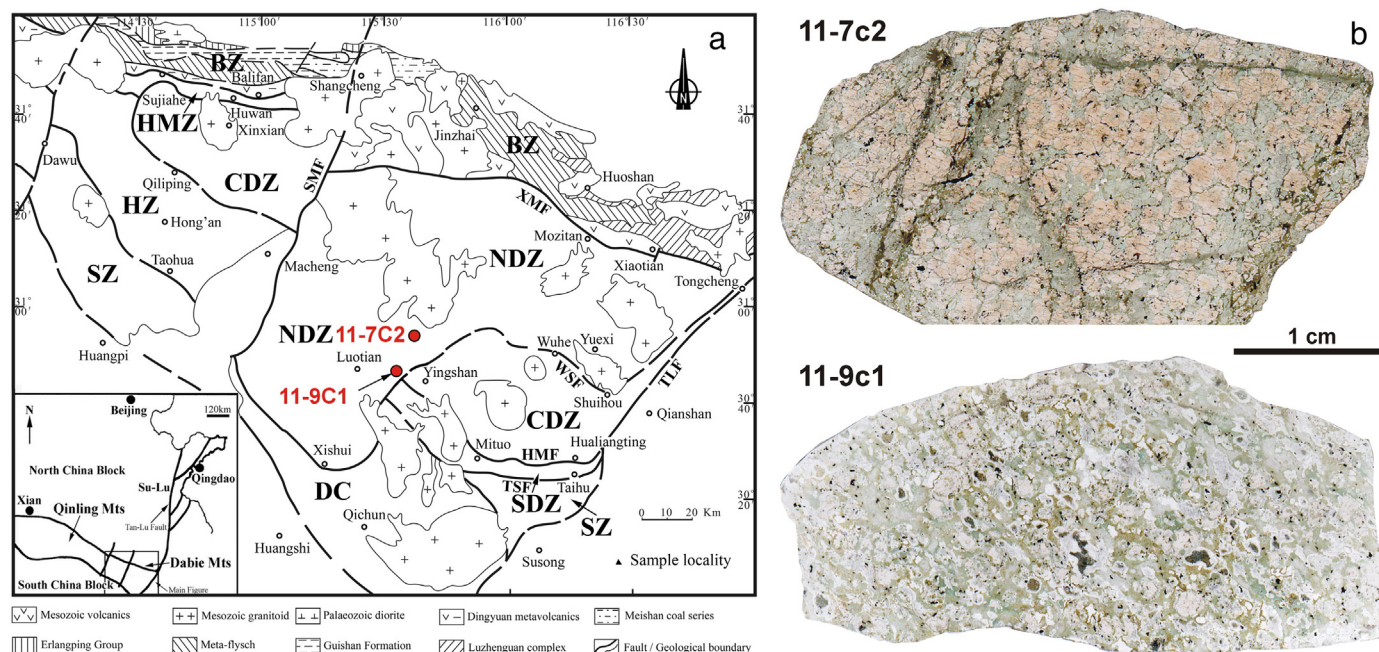


**Fig. 1.** (a) Schematic geological map of the Dabie orogen (modified from Liu et al., in press), with inset showing its location within the Triassic Qinling–Dabie–Sulu collision orogen in central China. Sample localities with sample numbers are reported in red. BZ, Beihuaiyang zone; NDZ, North Dabie complex Zone; CDZ, Central Dabie UHP metamorphic Zone; SDZ, South Dabie low-T eclogite Zone; SZ, Susong complex zone; HMZ, Huwan mélangé zone; HZ, Hong'an low-T eclogite zone; DC, amphibolite-facies Dabie complex; XMF, Xiaotian–Mozitan fault; WSF, Wuhe–Shuihou fault; HMF, Hualiangting–Mituo fault; TSF, Taihu–Shanlong fault; TLF, Tan–Lu fault; SMF, Shangcheng–Macheng fault. (b) Scanned overview of the two studied samples (thin sections). Note the zoned garnet (reddish core and pinkish rim) in sample 11-7c2, and the dark spot surrounded by a whitish corona (former kyanite now replaced by spinel + plagioclase symplectite) in sample 11-9c1.

of Earth Sciences, University of Torino. The operating conditions were: 50 s counting time and 15 kV accelerating voltage. SEM-EDS quantitative data (spot size = 2  $\mu\text{m}$ ) were acquired and processed using the Microanalysis Suite Issue 12, INCA Suite version 4.01; natural mineral standards were used to calibrate the raw data; the  $\Phi\rho Z$  correction (Pouchou and Pichoir, 1988) was applied. Mineral chemical data of representative minerals are reported in Fig. 5 and Tables SM6–SM7. Garnet, clinopyroxene, orthopyroxene and plagioclase compositions are expressed in terms of  $X_{\text{Ca}}$ ,  $X_{\text{Mg}}$ ,  $X_{\text{Mn}}$  and  $X_{\text{Na}}$ , defined as:  $X_{\text{Ca}} = \text{Ca}/(\text{Ca} + \text{Mg} + \text{Fe}^{2+} + \text{Mn})$ ,  $X_{\text{Mg}} = \text{Mg}/(\text{Ca} + \text{Mg} + \text{Fe}^{2+} + \text{Mn})$  and  $X_{\text{Mn}} = \text{Mn}/(\text{Ca} + \text{Mg} + \text{Fe}^{2+} + \text{Mn})$  for garnet,  $X_{\text{Na}} = \text{Na}/(\text{Na} + \text{Ca})$  for clinopyroxene,  $X_{\text{Mg}} = \text{Mg}/(\text{Mg} + \text{Fe}^{2+})$  for orthopyroxene and  $X_{\text{Ca}} = \text{Ca}/(\text{Ca} + \text{Na})$  for plagioclase.

Quantitative modal percentages of each mineral have been obtained by processing  $\mu\text{-XRF}$  maps of the whole thin sections with the software program “Petromod” (Cossio et al., 2002). The micro-XRF maps of the whole thin sections (Fig. SM1) were acquired using a  $\mu\text{-XRF}$  Eagle III-XPL spectrometer equipped with an EDS Si(Li) detector and with an Edax Vision32 microanalytical system (Department of Earth Sciences, University of Torino, Italy). The operating conditions were as follows: 100 ms counting time, 40 kV accelerating voltage and a probe current of 900  $\mu\text{A}$ . A spatial resolution of about 65  $\mu\text{m}$  in both x and y directions was used.

### 3.1. Sample 11-7c2

Sample 11-7c2 is a fine-grained eclogite mainly consisting of garnet (54 vol%) + clinopyroxene (27 vol%) + rutile (1 vol%), only slightly retrogressed in a plagioclase (8 vol%) + amphibole (9 vol%) + ilmenite (1 vol%) -bearing assemblage (Fig. 1b and Fig. SM1). Both garnet and clinopyroxene are strongly zoned.

Garnet crystals, up to 0.5 cm in diameter, show a dark red core (Grt<sub>1</sub>) and a pinkish rim (Grt<sub>2</sub>) (Fig. 2a). The dark-red Grt<sub>1</sub> may be divided in two domains (Fig. 4a): an inner core (Grt<sub>1a</sub>: 2 vol%), only locally

preserved, crowded of small inclusions of brown Cl-rich amphibole (Amp<sub>0</sub>, pargasite: Si = 6.0–6.1 a.p.f.u.;  $X_{\text{Na}} = 0.33\text{--}0.34$ ) and rutile, and an outer core (Grt<sub>1b</sub>: 9 vol%) with large clinopyroxene inclusions (Cpx<sub>1</sub>: Fig. 2a). The pinkish Grt<sub>2</sub> (43 vol%) is almost free of inclusions.  $X_{\text{Ca}}$  decreases from core to rim (Grt<sub>1a</sub>:  $X_{\text{Ca}} = 0.29\text{--}0.32$ ; Grt<sub>1b</sub>:  $X_{\text{Ca}} = 0.27\text{--}0.30$ ; Grt<sub>2</sub>:  $X_{\text{Ca}} = 0.27\text{--}0.29$ ), counterbalanced by an increase in  $X_{\text{Mg}}$  (Grt<sub>1a</sub>:  $X_{\text{Mg}} = 0.18\text{--}0.21$ ; Grt<sub>1b</sub>:  $X_{\text{Mg}} = 0.22\text{--}0.24$ ; Grt<sub>2</sub>:  $X_{\text{Mg}} = 0.24\text{--}0.26$ ).  $X_{\text{Mn}}$  is slightly higher in Grt<sub>1a</sub> than in Grt<sub>1b</sub> (Grt<sub>1a</sub>:  $X_{\text{Mn}} = 0.01\text{--}0.02$ ; Grt<sub>1b</sub>:  $X_{\text{Mn}} = 0.00\text{--}0.01$ ).

Three generations of clinopyroxene are distinguished on microstructural and chemical basis. Clinopyroxene inclusions in Grt<sub>1b</sub> are Na-rich augite (Cpx<sub>1</sub>: Jd<sub>11–14</sub>CaTs<sub>4–5</sub>Ac<sub>2–4</sub>Di<sub>60–62</sub>Hed<sub>18–19</sub>). Clinopyroxene in the matrix, up to few mm in length, is strongly zoned (Figs. 2b, c and 4a). Clinopyroxene core (Cpx<sub>2</sub>: 8 vol%) is an omphacite to Na-rich augite (Jd<sub>16–22</sub>CaTs<sub>0–1</sub>Ac<sub>0–4</sub>Di<sub>63–69</sub>Hed<sub>11–15</sub>) and contains coarse quartz + calcic amphibole (Amp<sub>3</sub>, edenite-pargasite: Si = 6.4–6.5 a.p.f.u.;  $X_{\text{Na}} = 0.27\text{--}0.31$ ) oriented lamellae (Fig. 2c, e, f) resembling the “hornblende with quartz caps” described by Page et al. (2005) and Anderson and Moecher (2007). Clinopyroxene rim (Cpx<sub>3</sub>: 19 vol%) is a Na-rich augite (Jd<sub>4–11</sub>CaTs<sub>4–7</sub>Ac<sub>1–4</sub>Di<sub>70–74</sub>Hed<sub>20–22</sub>) with fine orthopyroxene exsolution lamellae (Fig. 2c, d, f, h). The orthopyroxene lamellae are generally < 1  $\mu\text{m}$  in width; coarser orthopyroxene (Opx<sub>3</sub>:  $X_{\text{Mg}} = 0.61\text{--}0.65$ ) + plagioclase (Pl<sub>3</sub>:  $X_{\text{Ca}} = 0.23\text{--}0.33$ ) exsolutions are also locally observed (Fig. 2g). A discontinuous orthopyroxene rim is locally present around Cpx<sub>3</sub> (Fig. 2h).

Thin and discontinuous coronas of greenish amphibole + plagioclase + ilmenite develop at the interface between garnet (Grt<sub>2</sub>) and clinopyroxene (Cpx<sub>3</sub>) (Figs. 2b and 4a). Amphibole is a tschermakite (Si = 6.2–6.5 a.p.f.u.;  $X_{\text{Na}} = 0.28\text{--}0.31$ ) and plagioclase is mainly an andesine ( $X_{\text{Ca}} = 0.34\text{--}0.46$ ) although it is locally more calcic in the proximity of garnet ( $X_{\text{Ca}} = 0.57\text{--}0.80$ ). Ilmenite contains significant amounts of geikelite component (Ilm<sub>86</sub>Geik<sub>11</sub>Hem<sub>3</sub>).

Very rare quartz (< 1 vol%) is also present in the matrix (Fig. SM1), as discrete grains with homogeneous extinction. Quartz has not been

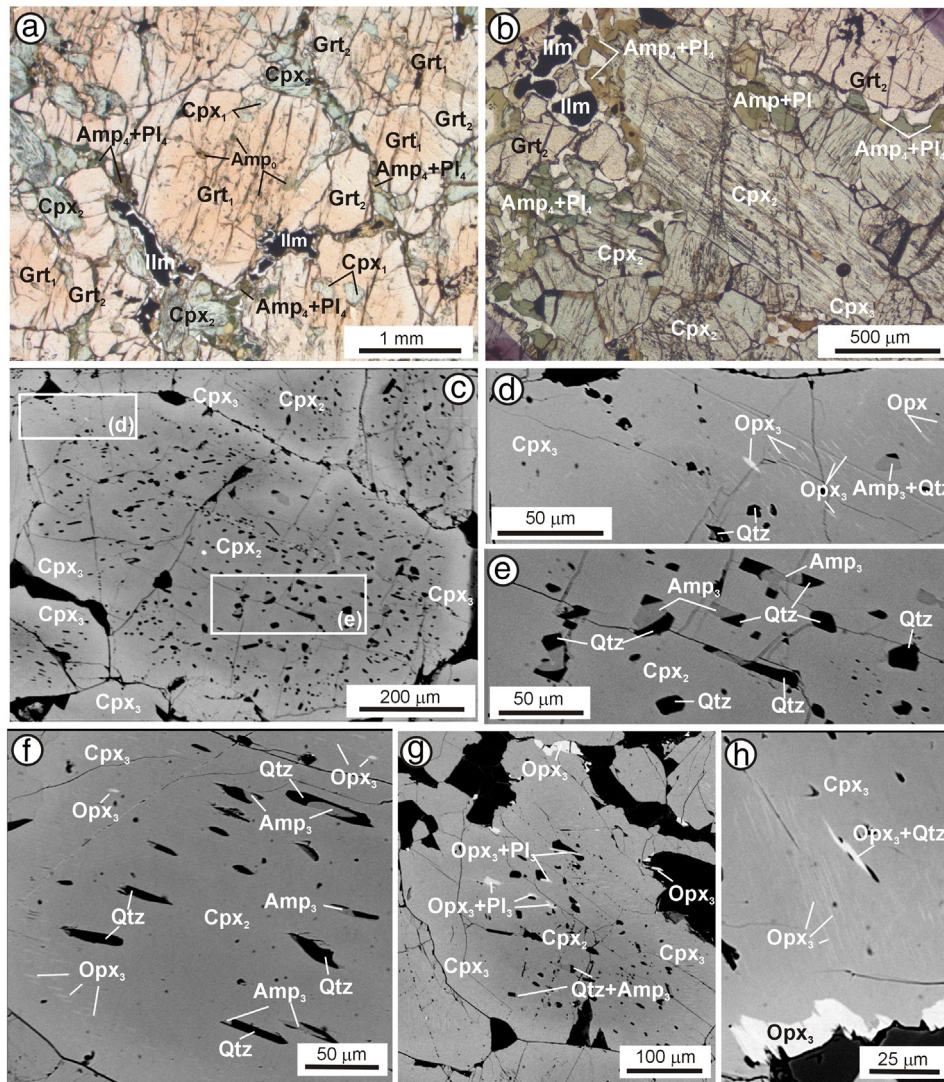


**Fig. 2.** Representative microstructures of sample 11-7c2. (a) Zoned garnet with a reddish core (Grt<sub>1</sub>) and a pinkish rim (Grt<sub>2</sub>). Grt<sub>1</sub> includes brown amphibole (Amp<sub>0</sub>) and green clinopyroxene (Cpx<sub>1</sub>). A discontinuous amphibole (Amp<sub>4</sub>) + plagioclase (Pl<sub>4</sub>) ± ilmenite corona separates garnet from matrix clinopyroxene. Plane Polarized Light (PPL). (b) Clinopyroxene of the matrix with coarse quartz + amphibole oriented lamellae. Clinopyroxene is partially replaced by greenish amphibole at its rim; a coarse-grained Amp<sub>4</sub> + Pl<sub>4</sub> ± Ilm corona is developed between clinopyroxene and garnet. PPL. (c) Zoned clinopyroxene: the core (Cpx<sub>2</sub>) includes coarse quartz + amphibole (Amp<sub>3</sub>) oriented lamellae, whereas the rim (Cpx<sub>3</sub>) contains fine orthopyroxene exsolutions. Back Scattered Electron image (BSE). (d) Detail of (c) showing the orthopyroxene oriented exsolutions (brighter in the BSE image) in Cpx<sub>3</sub>. BSE. (e) Detail of (c) showing the quartz + amphibole (Amp<sub>3</sub>) oriented lamellae in clinopyroxene core. BSE. (f) Zoned clinopyroxene with quartz + Amp<sub>3</sub> oriented lamellae in the core and Opx<sub>3</sub> exsolutions in the rim. BSE. (g) Zoned clinopyroxene with a large Cpx<sub>3</sub> rim including coarser Opx<sub>3</sub> + Pl<sub>3</sub> exsolutions. BSE. (h) Detail of Opx<sub>3</sub> exsolutions in Cpx<sub>3</sub>. Note the discontinuous Opx corona developed at the rim of clinopyroxene.

observed as inclusion within garnet or clinopyroxene, except for the coarse quartz + calcic amphibole oriented lamellae within clinopyroxene core (Cpx<sub>2</sub>).

### 3.2. Sample 11-9c1

Sample 11-9c1 is a quartz-kyanite ± zoisite/epidote-bearing eclogite pervasively retrogressed under granulite-facies conditions; it shows spectacular symplectitic and coronitic microstructures (Fig. 3a) and preserves few relics of the prograde and peak assemblages. It mainly consists of greenish amphibole (28 vol%), plagioclase (25 vol%), garnet (14 vol%), former kyanite now replaced by composite symplectites (10 vol%), quartz (10 vol%), clinopyroxene (6 vol%), orthopyroxene (6 vol%) and accessory ilmenite (2 vol%), magnetite and apatite (Fig. 1b and Fig. SM1).

Two different generations of garnet are distinguished based on microstructures and chemical composition. The first generation (Grt<sub>1</sub>) occurs as the core of mm-sized, fractured and strongly corroded, crystals

(Fig. 4b). It is characterized by relatively high Ca and low Mg contents (Grt<sub>1</sub>: X<sub>Ca</sub> = 0.19–0.25, X<sub>Mg</sub> = 0.34–0.39) and includes amphibole (Amp<sub>0</sub>: Si = 6.0–6.3 a.p.f.u.; X<sub>Na</sub> = 0.23–0.33), kyanite (replaced by a plagioclase + spinel symplectite and only rarely preserved), omphacite partially replaced by an amphibole + quartz symplectite, and rutile (Figs. 3b, c, e and 4b and SM1). Grt<sub>2</sub> occurs either as a discontinuous rim around Grt<sub>1</sub> (Fig. 4b) or as small (< 1 mm) grains in the matrix (Fig. 3a); it is always strongly corroded with the development of large embayments. Grt<sub>2</sub> is Mg-richer and Ca-poorer than Grt<sub>1</sub> (Grt<sub>2</sub>: X<sub>Ca</sub> = 0.13–0.20, X<sub>Mg</sub> = 0.39–0.45) and includes omphacite partially replaced by an amphibole + quartz symplectite (Fig. 3d, e), quartz, rutile and ilmenite. Grt<sub>2</sub> is locally overgrown by a discontinuous Grt<sub>3</sub> rim (Grt<sub>3</sub>: X<sub>Ca</sub> = 0.18–0.22, X<sub>Mg</sub> = 0.34–0.39) which shows rare orthopyroxene and plagioclase inclusions. X<sub>Mn</sub> is very low in all the garnet generations (X<sub>Mn</sub> < 0.02).

Omphacitic clinopyroxene (Cpx<sub>1</sub>: Jd<sub>26–35</sub>CaTs<sub>0–2</sub>Ac<sub>m0–4</sub>Di<sub>56–60</sub>Hed<sub>7–10</sub>) is rarely included in both Grt<sub>1</sub> and Grt<sub>2</sub>, where is partially replaced by an amphibole (Mg-hornblende) + quartz symplectite (Fig. 3d, e). 298



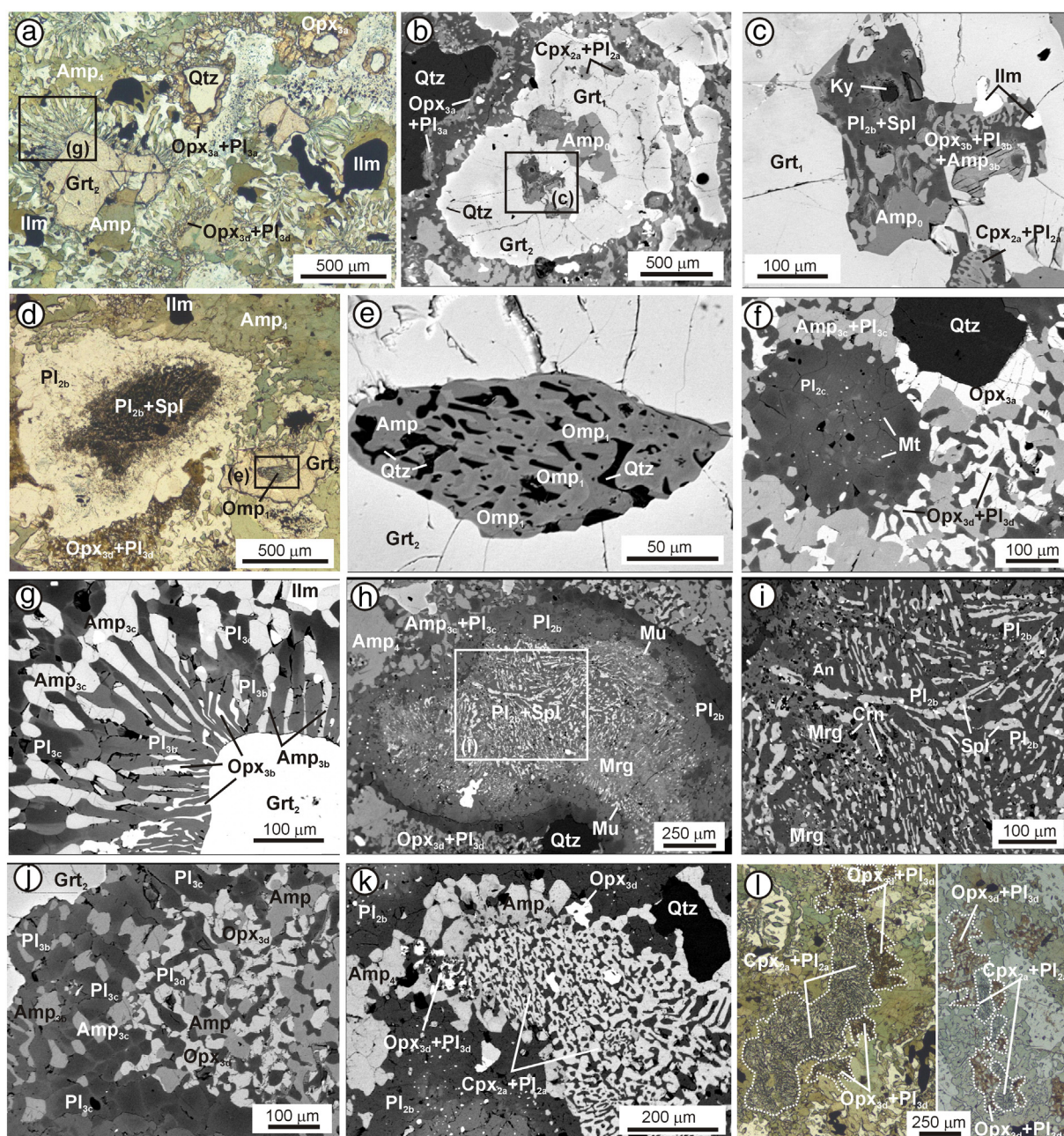


**Fig. 3.** Representative microstructures of sample 11-9c1. (a) Typical symplectitic and coronitic microstructures as seen at the optical microscope. Note the symplectitic corona around garnet (Grt<sub>2</sub>) and the pinkish orthopyroxene-bearing corona (Opx<sub>3a</sub> + Pl<sub>3a</sub>) around Qtz. PPL. (b) Zoned garnet with composite inclusions in the core (Grt<sub>1</sub>) and minor inclusions in the rim (Grt<sub>2</sub>). In the matrix, quartz is surrounded by an Opx<sub>3a</sub> + Pl<sub>3a</sub> corona. BSE. (c) Detail of (b) showing a composite inclusion in garnet core (Grt<sub>1</sub>). A kyanite relict is partially replaced by plagioclase (Pl<sub>2b</sub>) + minor spinel, whereas former omphacite is replaced by a Cpx<sub>2a</sub> + Pl<sub>2a</sub> symplectite. BSE. (d) Kyanite in the matrix is completely replaced by Pl<sub>2b</sub> + Spl symplectitic aggregates surrounded by a plagioclase corona. Note also the small garnet including omphacite on the right side of the image. PPL. (e) Detail of (d) showing an omphacite inclusion within garnet (Grt<sub>2</sub>), partially replaced by a symplectite of quartz + amphibole. BSE. (f) Roundish aggregate of plagioclase (Pl<sub>2c</sub>) + magnetite interpreted as pseudomorph after former epidote. Opx<sub>3d</sub> + Pl<sub>3d</sub> symplectites in the rock matrix and Opx<sub>3a</sub> corona around quartz are also evident. BSE. (g) Detail of (a) showing the composite symplectitic corona developed between garnet (Grt<sub>2</sub>) and the rock matrix. The inner corona consists of fine-grained vermicular Opx<sub>3b</sub> + Pl<sub>3b</sub> + Amp<sub>3b</sub> ± Ilm, whereas the outer corona is coarser-grained and consists of Amp<sub>3c</sub> + Pl<sub>3c</sub>. Note that the compositional discontinuity between Pl<sub>3b</sub> (brighter in the BSE image) and Pl<sub>3c</sub> (darker in the BSE image) is sharp and cuts through individual plagioclase grains. BSE. (h) Strongly zoned pseudomorph after kyanite. From core to rim the following assemblages are observed: Pl<sub>2b</sub> + Spl symplectite; Pl<sub>2b</sub> + Crn symplectite partially replaced by margarite; discontinuous corona of muscovite; inner plagioclase corona (An-rich: brighter in the BSE image); outer Pl corona (An-poor: darker in the BSE image). BSE. (i) Detail of (h) showing the inner portions of the pseudomorphs after kyanite. BSE. (j) Amp<sub>3b</sub> + Pl<sub>3b</sub> corona around garnet (on the left) and Opx<sub>3d</sub> + Pl<sub>3d</sub> symplectites in the matrix (on the right), BSE. (k, l) Cpx<sub>2a</sub> + Pl<sub>2a</sub> symplectites after former omphacite, partially overgrown by Opx<sub>3d</sub> + Pl<sub>3d</sub> symplectites, and later replaced by coarse grained Amp<sub>4</sub> at their rim. BSE (k) and PPL (l).

Omphacite is not preserved in the rock matrix, but is pervasively replaced by a clinopyroxene + plagioclase symplectite (Cpx<sub>2a</sub> + Pl<sub>2a</sub>; Figs. 3k, l and 4b). Symplectitic clinopyroxene (Cpx<sub>2a</sub>) is an augite with  $X_{Mg} = 0.69\text{--}0.71$ , and plagioclase is oligoclase to andesine (Pl<sub>2a</sub>:  $X_{Ca} = 0.25\text{--}0.35$ ).

Kyanite is not preserved except for very rare inclusions in Grt<sub>1</sub> (Fig. 3c); in the rock matrix it is completely replaced by a plagioclase +

spinel ± corundum symplectite that forms large pseudomorphs up to few mm in length (Fig. 3d, h). These pseudomorphs are strongly zoned, with a concentric arrangement of the different symplectitic domains (Fig. 3h). From core to rim the following assemblages are observed in the kyanite pseudomorphs (Fig. 3h, i): (i) spinel + plagioclase symplectite (Pl<sub>2b</sub> + Spl; Fig. 3i); spinel occurs as vermicular crystals hundreds of microns in length and belongs to the hercynite-spinel solid



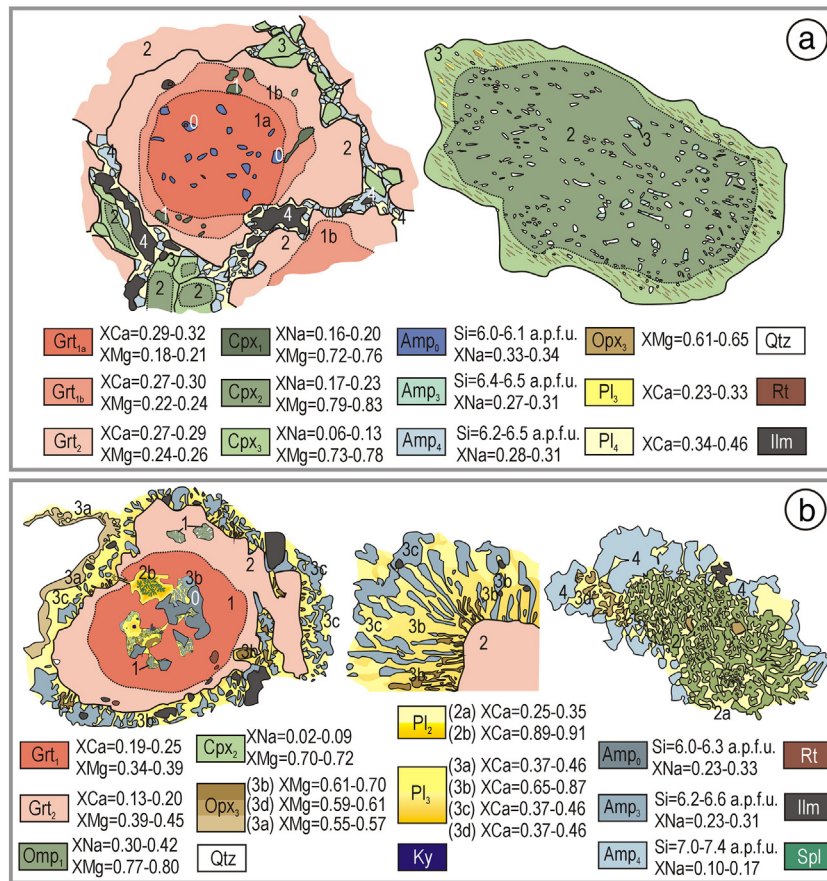


Fig. 4. Sketches of the main microstructural and compositional features of sample 11-7c2 (a) and 11-9c1 (b). Redrawn from Fig. 2a, c (a) and from Fig. 3b, g, k (b).

solution (Spl<sub>29-33</sub>), and plagioclase is almost pure anorthite (An<sub>89-90</sub>); (ii) plagioclase (An<sub>89-90</sub>) + corundum symplectite (Pl<sub>2b</sub> + Crn), partially replaced by margarite (Fig. 3i): in this domain, 50–100 μm thick, corundum is rarely preserved due to the pervasive overgrowth of margarite flakes; (iii) muscovite-bearing narrow and discontinuous corona (Fig. 3h): this domain may represent the hydration product of a primary assemblage no more preserved (e.g. sapphirine-bearing assemblage, in analogy with similar kyanite pseudomorphs described from the Variscides: Godard and Mabit, 1998); (iv) plagioclase corona (Fig. 3h): this domain consists of an inner plagioclase (An<sub>89-91</sub>) corona, ca. 100 μm thick, associated with small grains of Cr-rich magnetite, and an outer corona consisting of granoblastic plagioclase (An<sub>25-50</sub>). The contact between the inner and outer plagioclase corona is sharp and it is marked by the abrupt difference in the plagioclase composition. As described by Godard and Mabit (1998), this abrupt compositional discontinuity, not coinciding with grain boundaries (as it cuts through individual plagioclase grains) may represent the primary contact between kyanite and the matrix.

The presence of former zoisite/epidote is inferred due to the presence of granoblastic aggregates of plagioclase (An<sub>53-80</sub>) + fine-grained magnetite (Fig. 3f) (e.g. Giacomini et al., 2005).

Both Grt<sub>1</sub> and Grt<sub>2</sub> are pervasively replaced by a strongly zoned plagioclase + amphibole ± orthopyroxene symplectitic corona (Figs. 3a, b, g and 4b). Moving outward from garnet core, the following assemblages are observed: (i) orthopyroxene (Opx<sub>3b</sub>: X<sub>Mg</sub> = 0.61–0.70) + plagioclase (Pl<sub>3b</sub>: An<sub>65-87</sub>) + amphibole (Amp<sub>3b</sub>, tschermakite: Si = 6.2–6.6 a.p.f.u.; X<sub>Na</sub> = 0.23–0.31) ± ilmenite symplectite: both orthopyroxene and amphibole lamellae are oriented perpendicular to the garnet boundary and they increase in size outward (from few μm to tens of μm); (ii) coarser grained amphibole (Amp<sub>3c</sub>) + plagioclase (Pl<sub>3c</sub>: An<sub>37-46</sub>) ± ilmenite (Ilm<sub>88</sub>Geik<sub>4</sub>Hem<sub>7</sub>) symplectite: amphibole

(Amp<sub>3c</sub>) has approximately the same composition as that of the inner corona. In contrast, plagioclase composition changes abruptly passing from the inner to the outer corona, and this compositional discontinuity cuts through individual plagioclase grains (Fig. 3g).

Orthopyroxene-bearing coronas and symplectites occur in two additional microstructural positions: (i) as orthopyroxene (X<sub>Mg</sub> = 0.55–0.57) ± plagioclase (An<sub>37-46</sub>) corona around coarse-grained quartz (Opx<sub>3a</sub> + Pl<sub>3a</sub>: Figs. 3a, b, f and 4b), and (ii) as orthopyroxene (X<sub>Mg</sub> = 0.59–0.61) + plagioclase (An<sub>37-46</sub>) ± amphibole symplectites overgrowing the clinopyroxene + plagioclase symplectite after omphacite (Opx<sub>3d</sub> + Pl<sub>3d</sub>: Figs. 3j, k, l and 4b). These Opx<sub>3d</sub> + Pl<sub>3d</sub> symplectites do not form continuous coronas around the Cpx<sub>2a</sub> + Pl<sub>2a</sub> symplectites after omphacite because they are in turn overgrown by amphibole; however, their systematic occurrence at the rim of the Cpx<sub>2a</sub> + Pl<sub>2a</sub> symplectites (Fig. 3k, l) suggest that the Opx<sub>3d</sub> + Pl<sub>3d</sub> symplectites formed later than the Cpx<sub>2a</sub> + Pl<sub>2a</sub> symplectites.

Finally, a porphyroblastic greenish amphibole (Amp<sub>4</sub>, Mg-hornblende; Si = 7.0–7.4 a.p.f.u.; X<sub>Na</sub> = 0.10–0.17) overgrows the clinopyroxene + plagioclase symplectites after omphacite (Fig. 3k, l) and pervasively crystallizes in the rock matrix (Fig. 3a).

#### 4. Metamorphic evolution and reaction modelling

A complex metamorphic evolution, summarized in Fig. 6, may be inferred for the two studied samples based on microstructural observations and mineralogical analyses. Both samples show evidence of a prograde evolution from the HT amphibolite-facies up to HP (or UHP) eclogite-facies peak-P conditions, followed by a decompressional evolution down to low-P granulite-facies conditions. However, the two samples record different stages of this polyphasic metamorphic evolution. Sample 11-7c2 well preserves the prograde and peak-P

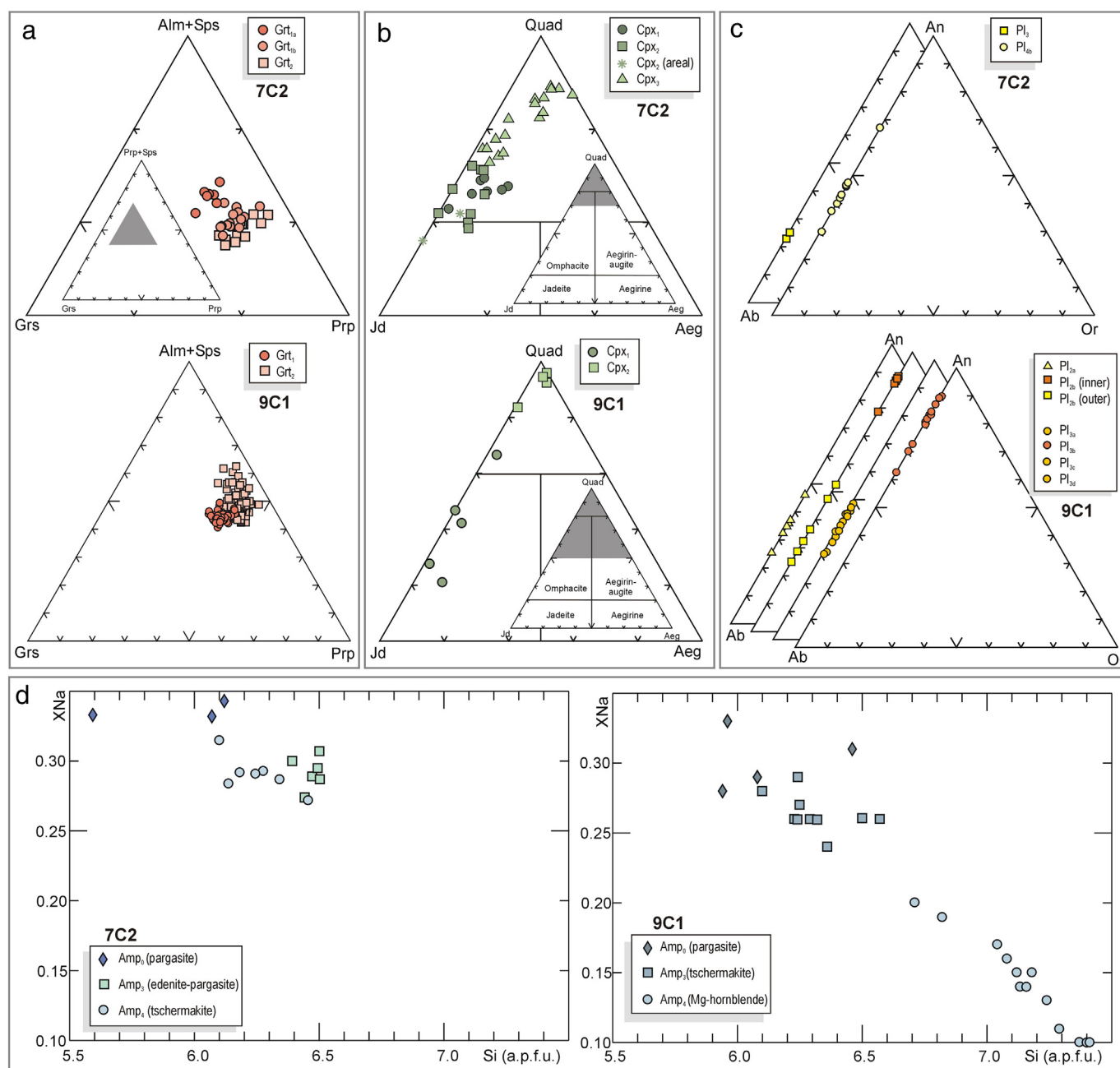


**Fig. 5.** Garnet (a), clinopyroxene (b), plagioclase (c) and amphibole (d) compositions plotted in the Grs-(Alm + Sps)-Prp, Jd-Quad-Aeg (Morimoto, 1988), Ab-An-Or and Si vs. X<sub>Na</sub> diagrams, respectively. Colours are the same as in Fig. 4.

assemblages and it was only slightly retrogressed during the following decompression at HT conditions; on the opposite, sample 11-9c1 shows few relics of the prograde and peak assemblages and it is dominated by reaction textures developed during decompression under granulite-facies conditions.

#### 4.1. Sample 11-7c2

##### 4.1.1. Assemblage 1

Prograde inclusions in the garnet core define the prograde assemblage Grt<sub>1</sub> + Cpx<sub>1</sub> ± Qtz + Rt. Brown amphibole (Amp<sub>0</sub>) is only included in the inner garnet core (Grt<sub>1a</sub>) and it may be interpreted as a prograde phase, stable prior to the Grt<sub>1</sub> growth. Overall, the modal percentage of the prograde assemblage 1 is very low (ca. 12 vol%).

##### 4.1.2. Assemblage 2

The same mineral phases, but with different compositions, also define the peak assemblage Grt<sub>2</sub> + Cpx<sub>2</sub> ± Qtz/Coe + Rt. Quartz is very rare and it is only observed in the rock matrix: it does not show evidence of derivation from former coesite (e.g. polycrystalline texture), but this evidence could have been obliterated during the following HT evolution. Therefore, the former presence of coesite at peak-P conditions cannot be ruled out.

Quartz oriented needles in clinopyroxene core (Cpx<sub>2</sub>) are generally considered as precipitation products from a Si-rich clinopyroxene precursor. Such inclusions are well-known in eclogites from several UHP terranes (e.g. Bakun-Czubarow, 1992; Dobrzynetskaia et al., 2002; Gayk et al., 1995; Janák et al., 2004; Katayama and Nakashima, 2003; Katayama et al., 2000; Liati et al., 2002; Page et al., 2005; Schmädicke and Müller, 2000; Smith, 1988, 2006; Song et al., 2003;



Sample 11-7c2				
PROGRADE STAGE (0)	PROGRADE STAGE (1)	HP/UHP STAGE (2)	DECOMPRESSION STAGE (3)	LATE HYDRATION STAGE (4)
Amp <sub>0</sub> (Ep) (Qtz) (Rt)	Grt <sub>1a</sub> → Grt <sub>1b</sub> Cpx <sub>1</sub> Qtz Rt	Grt <sub>2</sub> Cpx <sub>2</sub> Qtz/Coe Rt	(3a) Qtz + Amp <sub>3</sub> exsolutions in Cpx <sub>2</sub> core (3b) Cpx <sub>3</sub> with Opx <sub>3</sub> + Pl <sub>3</sub> exsolutions (replacing Cpx <sub>2</sub> at the rim) Ilm	Amp <sub>4</sub> + Pl <sub>4</sub> (+Ilm) corona between Grt <sub>2</sub> and Cpx <sub>3</sub> Ilm

Sample 11-9c1				
PROGRADE STAGE (0)	HP/UHP STAGE (1)	EARLY DECOMPRESSION STAGE (2)	LATE DECOMPRESSION STAGE (3)	LATE HYDRATION STAGE (4)
Amp <sub>0</sub> (Pl <sub>0</sub> )? (Pa) (Ep) Qtz (Ilm)	Grt <sub>1</sub> Cpx <sub>1</sub> Ky (Zo) Qtz/Coe Rt	Grt <sub>2</sub> Cpx <sub>2a</sub> + Pl <sub>2a</sub> symplectite Pl <sub>2b</sub> + Spl ± Crn symplectite Pl <sub>2c</sub> Qtz Ilm	(3a) Opx <sub>3a</sub> + Pl <sub>3a</sub> corona around Qtz (3b) Opx <sub>3b</sub> + Pl <sub>3b</sub> + Amp <sub>3b</sub> symplectitic inner corona around Grt (3c) Pl <sub>3c</sub> + Amp <sub>3c</sub> symplectitic outer corona around Grt (3d) Opx <sub>3d</sub> + Pl <sub>3d</sub> symplectite overgrowing Cpx <sub>2a</sub> + Pl <sub>2a</sub> symplectite	Amp <sub>4</sub>

**Fig. 6.** Metamorphic evolution inferred for samples 11-7c2 and 11-9c1. Minerals in brackets are not preserved and their former presence is inferred basing on microstructural considerations.

Terry et al., 2000; Tsai and Liou, 2000; Zhang and Liou, 1998; Zhang et al., 2002, 2003, 2005, 2007; Zhu and Ogasawara, 2002) and were initially taken as UHP-indicators (e.g. Katayama et al., 2000; Smyth, 1980; Zhang et al., 2005). However, the interpretation of these microstructures is already highly debated (e.g. Dobrzhinetskaya and Faryad, 2011 and references therein), with evidence either supporting the univocal UHP stability of the supersilicic clinopyroxene precursor (e.g. Zhao et al., 2011) or against it (e.g. Konzett et al., 2008; Page et al., 2005). Furthermore, Proyer et al. (2009) recently interpreted similar oriented precipitates of quartz and amphibole in clinopyroxene from the Greek Rhodope as the products of an open system precipitation during eclogite-granulite-amphibolite transition, thus suggesting that no prior Ca-Eskola -rich omphacite is required to explain these microstructures. The occurrence of quartz ± amphibole oriented lamellae within Cpx<sub>2</sub> cannot be therefore considered as an unequivocal evidence of the attainment of UHP conditions.

#### 4.1.3. Assemblage 3

In this sample, evidence of decompression at granulite-facies conditions is limited to few orthopyroxene-bearing microstructures: (i) the Opx<sub>3</sub> ± Pl<sub>3</sub> oriented lamellae within clinopyroxene rim, and (ii) thin and discontinuous orthopyroxene rim around clinopyroxene. Similar microstructures were described Anderson and Moecher (2007) for eclogites from the Appalachian Blue Ridge and by Xiao et al. (2001) for garnet clinopyroxenites from the North Dabie Zone, and were interpreted as evidence of granulite-facies overprinting, but the origin of such exsolution microstructures remains ambiguous.

#### 4.1.4. Assemblage 4

Additional evidence of the post-peak re-equilibration in this sample is limited to minor Pl<sub>4</sub> + Amp<sub>4</sub> + Ilm<sub>4</sub> discontinuous, coarse-grained, symplectitic coronas between garnet (Grt<sub>2</sub>) and clinopyroxene (Cpx<sub>3</sub>); microstructural relationships indicate that the development of these coronas was later than the Cpx<sub>3</sub> growth, thus suggesting that assemblage 4 represents a late hydration stage.

### 4.2. Sample 11-9c1

#### 4.2.1. Assemblage 1

Prograde relics are very scarce and limited to amphibole inclusions (Amp<sub>0</sub>) in garnet cores. The peak-P assemblage 1 is represented by Grt<sub>1</sub> + Omp<sub>1</sub> + Ky + Ep + Qtz/Coe + Rt. Kyanite is only rarely

preserved as inclusion in Grt<sub>1</sub>, whereas the former occurrence of epidote in the peak assemblage is inferred from its pseudomorphs consisting of granoblastic plagioclase + fine-grained magnetite. Quartz has not been observed included in Grt<sub>1</sub>; quartz in the matrix does not show microstructural evidence of derivation from former coesite, but the former stability of coesite in the peak-P assemblage cannot be ruled out due to the pervasive re-equilibration at HT conditions that may have obliterated the evidence of coesite breakdown, as observed in other UHP terranes (e.g. Lang and Gilotti, 2007). The modal percentage of the preserved peak-P assemblage 1 is very low (< 10 vol%).

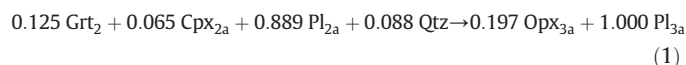
#### 4.2.2. Assemblage 2

The modally dominant assemblage consists of Grt<sub>2</sub> + Cpx<sub>2a</sub> + Pl<sub>2a</sub> symplectite after omphacite + Pl<sub>2b</sub> + Spl ± Crn symplectite after kyanite + Pl<sub>2c</sub> + Mt pseudomorphs after epidote + Qtz + Ilm. Assemblage 2 reflects a pervasive re-equilibration of the peak-P assemblage 1 under high-P granulite-facies conditions. Clinopyroxene + plagioclase intergrowths after omphacite associated with plagioclase + spinel ± corundum ± sapphirine symplectites after kyanite are relatively common in kyanite-bearing eclogites of different ages and from different HP/UHP terranes that experienced nearly isothermal exhumation at HT (e.g. the Sveconorwegian orogen in south-west Scandinavia: Möller, 1999; the Canadian Shield: Baldwin et al., 2007; the Greenland Caledonides: Elveland and Gilotti, 2000; the Variscan terranes of central and southern Europe, such as the Armorican Massif, the Bohemian Massif and the northern Sardinia: Giacomini et al., 2005; Godard and Mabit, 1998; Nakamura et al., 2004; O'Brien, 1989, 1997; Okrusch et al., 1991; the Su-Lu region in eastern China: Nakamura and Hirajima, 2000). Both microstructural observations and material transfer modelling generally suggest that kyanite and omphacite breakdowns were coupled (Godard and Mabit, 1998; Möller, 1999): the kyanite and omphacite pseudomorphs exchanged components during their formation, behaving as a local metasomatic system at a microscopic scale. In the studied sample 11-9c1, the growth of the Mg-rich Grt<sub>2</sub> is likely linked to the omphacite and kyanite breakdown: the local occurrence of omphacite relics (only slightly retrogressed in an amphibole + quartz symplectite) included in Grt<sub>2</sub> provides evidence that Grt<sub>2</sub> began to grow prior to the complete breakdown of omphacite. As a consequence, omphacite and kyanite breakdowns and Grt<sub>2</sub> growth most likely involved the whole rock volume (i.e. closed-system behaviour; see also Godard and Mabit, 1998), although they define local microdomains.

### 4.2.3. Assemblage 3

Later orthopyroxene-bearing assemblages are confined to coronitic and symplectitic microdomains which represent reaction textures developed under low-P granulite-facies conditions. Some of these microstructures (i.e. assemblages 3a and 3d) are homogeneous in composition, whereas others are clearly zoned (i.e. assemblages 3b and 3c).

**4.2.3.1. Assemblage 3a.** A  $\text{Opx}_{3a} \pm \text{Pl}_{3a}$  symplectitic corona separates quartz from both garnet and the  $\text{Cpx}_{2a} + \text{Pl}_{2a}$  symplectite, thus suggesting that it formed through a reaction between quartz and garnet +  $\text{Cpx}_{2a} + \text{Pl}_{2a}$  symplectite. Reaction modelling by the least square method (freeware application available on demand; Godard, 2009) applied to the composition of  $\text{Grt}_2$ ,  $\text{Cpx}_{2a}$ ,  $\text{Pl}_{2a}$ ,  $\text{Opx}_{3a}$  and  $\text{Pl}_{3a}$  yielded the following balanced reaction accounting for the formation of the  $\text{Opx}_{3a} \pm \text{Pl}_{3a}$  corona around quartz:



It is underlined that metamorphic reactions balanced using the method of least squares can be considered satisfactory if (a) the results are consistent with the observed microstructures (i.e. inferred reactants and products should appear on opposite sides of the model reaction), and (b) the residuals (i.e. molar bulk composition of the products - molar bulk composition of the reactants) are low (e.g. (Adjerid et al., 2013; Cruciani et al., 2008 for further details on the method). The mineral compositions used, the resulting stoichiometric coefficients and the residuals are reported in Table 1.

**4.2.3.2. Assemblages 3b and 3c.** Garnet is surrounded by a double symplectitic corona: the inner corona, adjacent to garnet, consists of  $\text{Opx}_{3b} + \text{Pl}_{3b} + \text{Amp}_{3b} \pm \text{Ilm}$ , whereas the outer corona, adjacent to the  $\text{Cpx}_{2a} + \text{Pl}_{2a}$  symplectite in the rock matrix, consists of  $\text{Pl}_{3c} + \text{Amp}_{3c} \pm \text{Ilm}$ . The abrupt discontinuity in the plagioclase composition between the inner and outer corona cuts through individual plagioclase grains, thus defining a “front” that separates a Ca-rich, Na-poor domain from a Ca-poor, Na-rich domain. This compositional

discontinuity may therefore represent the primary contact between garnet and the  $\text{Cpx}_{2a} + \text{Pl}_{2a}$  symplectite (e.g. Godard and Mabit, 1998). This is typical of metasomatic zoning in which the discontinuities correspond to diffusion fronts propagating from rim to core (e.g. Guy, 1984, 1993; Korzhinskii, 1970). According to the assumption of local (mosaic) equilibrium (Korzhinskii, 1970), all corona layers (with sharp zone's fronts) are supposed to be formed simultaneously, and with time they increase in size without changing their mineral composition. The diffusion proceeds due to gradients in the chemical potentials of the diffusing components in an intergranular fluid. Therefore, according to this model, it is likely that the inner and outer coronas surrounding garnet formed simultaneously and were stable at the same time, and that the differences in plagioclase composition and the sequences of the coronas between garnet and  $\text{Cpx}_{2a} + \text{Pl}_{2a}$  symplectite depend on different chemical potential gradients at the corona interfaces. The presence of amphibole in both the corona's layers confirms the hypothesis that the corona growth took place through the fluid phase, not only by solid-solid phase diffusion (e.g. Larikova and Zarakisky, 2009). Modelling of the reactions involved in the simultaneous growth of the two corona's layers is difficult because each chemical component diffuses at different speed (e.g. Proyer et al., 2014), and because the existence of two different layers imply that the chemical potential gradients of the diffusing components were not completely reset during the metamorphic evolution.

**4.2.3.3. Assemblage 3d.**  $\text{Opx}_{3d} + \text{Pl}_{3d}$  symplectites locally overgrow the  $\text{Cpx}_{2a} + \text{Pl}_{2a}$  symplectite in the rock matrix. The formation of these symplectites may be explained by the following balanced reaction (the mineral compositions used, the resulting stoichiometric coefficients and the residuals are reported in Table 1):



### 4.2.4. Assemblage 4

A pervasive growth of porphyroblastic amphibole ( $\text{Amp}_4$ ) occurred in the rock matrix, especially on the  $\text{Cpx}_{2a} + \text{Pl}_{2a}$  symplectite domains but also on other microstructural sites, partially obliterating the relationships between the earlier reaction textures. The growth of  $\text{Amp}_4$

**Table 1**  
Mass balance of the reactions.

Sample 11-9c1 – Assemblage 3a (Opx <sub>3a</sub> + Pl <sub>3a</sub> symplectitic corona around Qtz)											
Reactants					Products			Σreact	Σprod	Residuals	
Phases	Grt <sub>2</sub>	Cpx <sub>2a</sub>	Pl <sub>2a</sub>	Qtz	Phases	Opx <sub>3a</sub>	Pl <sub>3a</sub>				
coeff	0.125	0.065	0.889	0.088	coeff	0.197	1.000				
SiO <sub>2</sub>	2.99	1.96	2.68	1.00	SiO <sub>2</sub>	1.98	2.58	SiO <sub>2</sub>	2.970	2.970	0.000
Al <sub>2</sub> O <sub>3</sub>	0.98	0.03	0.65	0.00	Al <sub>2</sub> O <sub>3</sub>	0.01	0.70	Al <sub>2</sub> O <sub>3</sub>	0.702	0.702	0.000
CaO	0.44	0.90	0.35	0.00	CaO	0.02	0.42	CaO	0.425	0.424	-0.001
Na <sub>2</sub> O	0.00	0.03	0.33	0.00	Na <sub>2</sub> O	0.00	0.29	Na <sub>2</sub> O	0.291	0.290	-0.001
MgO	1.33	0.73	0.00	0.00	MgO	1.09	0.00	MgO	0.214	0.215	0.001
FeO	1.23	0.30	0.00	0.00	FeO	0.87	0.00	FeO	0.173	0.172	-0.002
Sample 11-9c1 – Assemblage 3d (Opx <sub>3d</sub> + Pl <sub>3d</sub> symplectites)											
Reactants				Products			Σreact	Σprod	Residuals		
Phases	Cpx <sub>2a</sub>	Pl <sub>2a</sub>		Phases	Opx <sub>3d</sub>	Pl <sub>3d</sub>					
coeff	0.110	0.940		coeff	0.082	1.000					
SiO <sub>2</sub>	1.96	2.68		SiO <sub>2</sub>	1.97	2.55	SiO <sub>2</sub>	2.734	2.712	-0.023	
Al <sub>2</sub> O <sub>3</sub>	0.03	0.65		Al <sub>2</sub> O <sub>3</sub>	0.02	0.71	Al <sub>2</sub> O <sub>3</sub>	0.614	0.711	0.097	
CaO	0.90	0.35		CaO	0.02	0.45	CaO	0.428	0.452	0.024	
Na <sub>2</sub> O	0.03	0.33		Na <sub>2</sub> O	0.00	0.28	Na <sub>2</sub> O	0.308	0.275	-0.033	
MgO	0.73	0.00		MgO	1.17	0.00	MgO	0.080	0.096	0.016	
FeO	0.30	0.00		FeO	0.78	0.00	FeO	0.033	0.064	0.031	

Reactions were balanced using the least-squares method (see “Metamorphic evolution and reaction modelling” in the text). Stoichiometric coefficients and compositions are expressed in moles.  $\Sigma_{\text{react}}$ : overall composition of the reactants;  $\Sigma_{\text{prod}}$ : overall composition of the products; *Residuals*: residual vector from the method of least squares (molar bulk composition of the product - molar bulk composition of the reactants).

likely reflects a pervasive hydration of the earlier, almost anhydrous, assemblages.

## 5. Thermodynamic modelling

### 5.1. Strategy for calculating the effective bulk compositions

Symplectitic and coronitic reaction textures are present in both the samples, although more widespread in sample 11-9c1. These reaction textures are the evidence that textural and compositional equilibrium was attained only on a domainal scale and allow the qualitative reconstruction of the complex metamorphic history of these rocks (Fig. 6). However, the lack of textural equilibrium represents a challenge for the petrological modelling of the P–T evolution, which is based on the assumptions of equilibrium thermodynamic. The identification of the effectively reacting equilibration volumes is, in this case, fundamental to ensure the success of the modelling (Powell and Holland, 2008).

The whole P–T evolution of the studied samples was reconstructed using the pseudosection approach. The effectively reacting equilibration volumes (i.e. the input bulk compositions for each pseudosection) were chosen according to the following strategy:

- The measured bulk-rock compositions were used to model the prograde to peak-P histories of both samples, prior to the development of symplectitic and coronitic textures (i.e. sample 11-7c2: assemblages 1 and 2; sample 11-9c1: assemblage 1). Whole-rock bulk compositions were calculated as the average of 30 SEM-EDS analyses of 4.70 mm × 3.20 mm areas (Table 2).
- The measured bulk-rock composition was also used to model the growth of assemblage 2 in sample 11-9c1, because microstructural evidence suggests that omphacite and kyanite breakdowns were linked to the growth of Grt<sub>2</sub> and that the whole rock volume was therefore involved in this stage (i.e. closed-system behaviour; see also Godard and Mabit, 1998);
- The composition of the effectively reacting microdomains that were involved in the formation of symplectites and coronae (sample 11-9c1: assemblages 3a and 3d; Table 2) was calculated according to the method of Cruciani et al. (2012) and Adjerid et al. (2013) (see also Cruciani et al., 2008, 2011; Godard, 2009; Groppo et al., 2007a,b; Langone et al., 2009), basing on mineral compositions and the stoichiometric coefficients of the previously discussed balanced reactions (i.e. total bulk composition of the products; Table 1). The modelling of each microdomain can be considered reliable if: (a) the modelled pseudosection shows a P–T field with the reactants (with almost null quantities for the products) and another with the products (with almost null quantities for the reactants); (b) the compositional isopleths of the products intersect in the multivariant field that precisely corresponds to the transition between reactants and products,

and (c) if some of the domainal microstructures show mutual relationships suggesting their contemporaneous growth, the P–T constraints obtained from the two different pseudosections should be the same.

### 5.2. Pseudosection calculation

Pseudosections have been calculated using Perplex 6.6.6 (version May 2013 – Connolly, 1990, 2009) and the internally consistent thermodynamic dataset and equation of state for H<sub>2</sub>O of Holland and Powell (1998, revised 2004). The minerals considered in the calculation were: garnet, omphacite, amphibole, orthopyroxene, plagioclase, epidote, quartz, kyanite, sillimanite, rutile, ilmenite, magnetite and hematite. The following solid solution models were used: garnet (Holland and Powell, 1998), clinopyroxene (Green et al., 2007), amphibole (Dale et al., 2005), orthopyroxene (Powell and Holland, 1999), plagioclase (Newton et al., 1980), epidote (Holland and Powell, 1998).

## 6. Results

### 6.1. Prograde evolution of sample 11-7c2

A P–T pseudosection was calculated in the MnNCFMASTHO system using the measured whole rock bulk composition of sample 11-7c2 (Table 2). A Fe<sub>2</sub>O<sub>3</sub>/(FeO + Fe<sub>2</sub>O<sub>3</sub>) ratio (X<sub>Fe<sub>2</sub>O<sub>3</sub></sub>) of 0.05 was imposed, considering the low amount of Fe<sup>+3</sup>-bearing minerals occurring in this sample (1 vol% of ilmenite with Hem<sub>3</sub>; 27 vol% of Cpx with Ac<sub>m0-4</sub>). The calculated P–T pseudosection is dominated by 5- and 6-variant fields at P < 15 kbar, whereas a large 7-variant field occurs at P > 15 kbar (Fig. 7a). The main phase-in and phase-out boundaries are reported in Fig. 8, that also shows the variation in modal amounts of the main mineral phases.

#### 6.1.1. Assemblage 1

Prograde assemblage 1 (Grt<sub>1</sub> + Cpx<sub>1</sub> + Qtz ± Amp + Rt) is modelled by a narrow 6-variant field at 600–720 °C, 12–23 kbar. Further information are given by the comparison between the modelled compositional isopleths and the measured garnet composition (Grt<sub>1a</sub>: X<sub>Mg</sub> = 0.18–0.21, X<sub>Ca</sub> = 0.29–0.32; Grt<sub>1b</sub>: X<sub>Mg</sub> = 0.22–0.24, X<sub>Ca</sub> = 0.27–0.30), which constrain the growth of Grt<sub>1a</sub> and Grt<sub>1b</sub> at 640–700 °C, 12–15 kbar and 650–710 °C, 14–17 kbar, respectively (Fig. 7a and SM2). The modelled X<sub>Na</sub>(Cpx) and X<sub>Mg</sub>(Cpx) isopleths constrain the growth of Cpx<sub>1</sub> (X<sub>Na</sub> = 0.19–0.24, X<sub>Mg</sub> = 0.72–0.76) at slightly lower P conditions with respect to the growth of Grt<sub>1</sub>, in the Grt + Cpx + Qtz + Amp + Ep + Rt 5-variant field (Fig. SM2).

#### 6.1.2. Assemblage 2

Peak assemblage 2 (Grt<sub>2</sub> + Cpx<sub>2</sub> + Qtz + Rt) is modelled by the large 7-variant field at P > 15 kbar. The modelled compositional isopleths of garnet (X<sub>Mg</sub> = 0.24–0.26, X<sub>Ca</sub> = 0.27–0.29) and clinopyroxene (X<sub>Na</sub> = 0.17–0.23, X<sub>Mg</sub> = 0.79–0.83) constrain the P–T conditions at which Grt<sub>2</sub> and Cpx<sub>2</sub> grew at 670–830 °C, > 16 kbar (Fig. 7a and SM2). Pressure conditions cannot be constrained with further precision, due to the almost insensitivity of garnet and clinopyroxene compositions to pressure variations.

Overall, the prograde evolution of sample 11-7c2 is characterized by an increase of both P and T from about 650 °C, 12 kbar up to peak-P conditions of > 700 °C, > 16 kbar. A maximum amount of 58 vol% of garnet and 39 vol% of clinopyroxene is modelled at this peak stage, and a continuous growth of both these phases is predicted by the modelled isomodes (Fig. 8).

**Table 2**  
Whole-rock and effective bulk compositions (wt%) for pseudosection calculation.

Sample	11-7c2	11-9c1				
Assemblage	1a, 1b, 2	XFe <sub>2</sub> O <sub>3</sub> = 0	XFe <sub>2</sub> O <sub>3</sub> = 1	1, 2	3a	3d
	Fig. 7a	Fig. 7b	Fig. 7b	Fig. 7c	Fig. 10a	Fig. 10c
SiO <sub>2</sub>	44.73	51.31	51.31	51.31	57.06	56.84
TiO <sub>2</sub>	1.52	1.08	1.08	1.08		
Al <sub>2</sub> O <sub>3</sub>	15.23	18.70	18.70	18.70	22.88	25.32
Fe <sub>2</sub> O <sub>3</sub>	0.80		10.00	4.50		
FeO	15.22	10.00	0.00	5.50	3.94	1.60
MnO	0.20	0.00	0.00	0.00	0.00	0.00
MgO	8.04	6.41	6.41	6.41	2.77	1.35
CaO	13.00	9.73	9.73	9.73	7.60	8.84
Na <sub>2</sub> O	1.27	2.77	2.77	2.77	5.75	6.05
Total	100.00	100.00	100.00	100.00	100.00	100.00



## 6.2. Prograde evolution of sample 11-9c1

A P-T pseudosection was calculated in the NCFMASTHO system using the measured whole rock bulk composition of sample 11-9c1 (Table 2). MnO was neglected because it is present in very low amounts in all the mineral phases. The estimate of  $X_{Fe_2O_3}$  for this sample is more crucial than the previous one, because the amount of  $Fe^{+3}$ -bearing minerals is relatively high (28 vol% of amphibole with an average

$X_{Fe_2O_3} = 0.10$ , 2 vol% of ilmenite with Hem<sub>7</sub>, and minor magnetite and spinel). In order to constrain the  $X_{Fe_2O_3}$  in the whole rock bulk composition, a P- $X_{Fe_2O_3}$  pseudosection (Fig. 7b) was calculated at 750 °C and 800 °C (i.e. T at peak-P conditions constrained from sample 11-7c2). The stability field of the observed peak assemblage 1 (Grt<sub>1</sub> + Omp<sub>1</sub> + Ky + Ep + Qtz + Rt) combined with the Grt<sub>1</sub> composition (modelled isopleths of  $X_{Mg} = 0.34$ –0.39;  $X_{Ca} = 0.19$ –0.25) allow constraining an  $X_{Fe_2O_3} = 0.45$  for this sample (Fig. 7b).

The calculated P-T pseudosection (Fig. 7c) is dominated by 2-, 3- and 4-variant fields at  $P < 15$  kbar, whereas a large 4-variant field occurs at  $P > 15$  kbar. The main phase-in and phase-out boundaries are reported in Fig. 9, that also shows the variation in modal amounts of the main mineral phases.

## 6.2.1. Assemblage 1

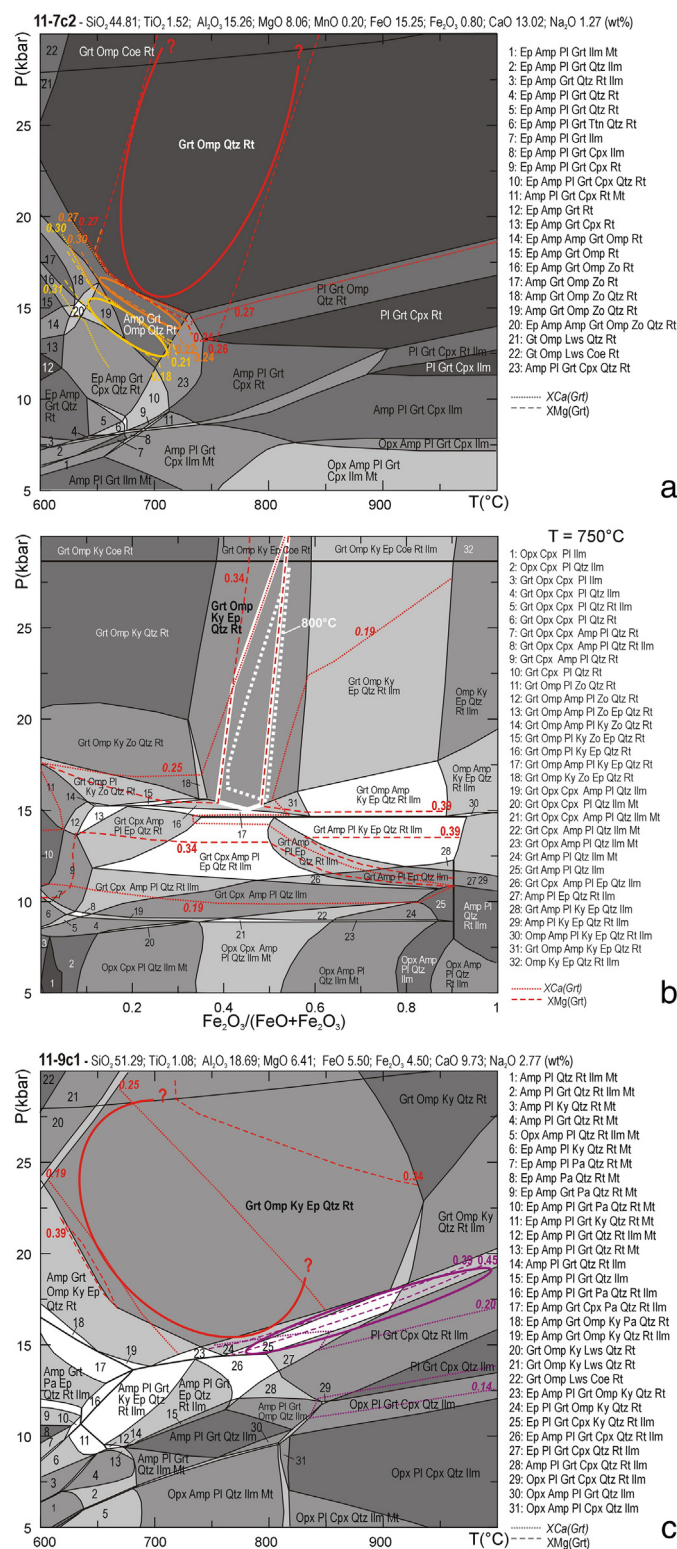
Peak assemblage 1 (Grt<sub>1</sub> + Omp<sub>1</sub> + Ky + Ep + Qtz + Rt) is modelled by a large 4-variant field at  $T < 930$  °C,  $P > 15$  kbar. The modelled compositional isopleths of garnet ( $X_{Mg} = 0.34$ –0.39,  $X_{Ca} = 0.19$ –0.25) constrain the growth of Grt<sub>1</sub> at 650–850 °C, 15–28 kbar (Fig. 7c); these isopleths are widely spaced in this field assemblage and have the same trend (Fig. SM3), this is why the P-T conditions of Grt<sub>1</sub> growth are not tightly constrained. Furthermore, these P-T conditions likely represent minimum P-T conditions for the Grt<sub>1</sub> growth, because Grt<sub>1</sub> was partially resorbed prior to the Grt<sub>2</sub> formation. The modelled  $X_{Na}(Cpx)$  isopleths in this field ( $X_{Na} = 0.40$ –0.44) (Fig. SM3) are in agreement with the maximum  $X_{Na}$  measured in the rare omphacite inclusions preserved within garnet ( $X_{Na} = 0.42$ ).

A maximum amount of 49 vol% of clinopyroxene, 22 vol% of garnet, 17 vol% of kyanite, 11 vol% of quartz and 7 vol% of epidote is modelled at this peak-P stage (Fig. 9).

## 6.3. Decompressional evolution of sample 11-9c1

## 6.3.1. Assemblage 2

This assemblage (Grt<sub>2</sub> + Cpx<sub>2a</sub> + Pl<sub>2a</sub> symplectite after omphacite + Pl<sub>2b</sub> + Spl ± Crn symplectite after kyanite + Pl<sub>2c</sub> + Mt pseudomorphs after zoisite/epidote + Qtz + Ilm) is the result of the breakdown of omphacite, kyanite and epidote that occurred simultaneously with the growth of Grt<sub>2</sub>; it was therefore modelled using the same P-T pseudosection used to model the peak-P assemblage 1, because the whole rock bulk composition is representative of the effective reactive volume during this stage. The modelled modal amounts of mineral phases (Fig. 9) are coherent with microstructural observations and show that Grt<sub>2</sub> grew at  $T > 800$  °C in a narrow P interval of ca. 2 kbar between 15 and 20 kbar depending on T. The growth of Grt<sub>2</sub> coincides with the breakdown of omphacite, kyanite and zoisite/epidote, as well as with the transition of rutile to ilmenite. The modelled



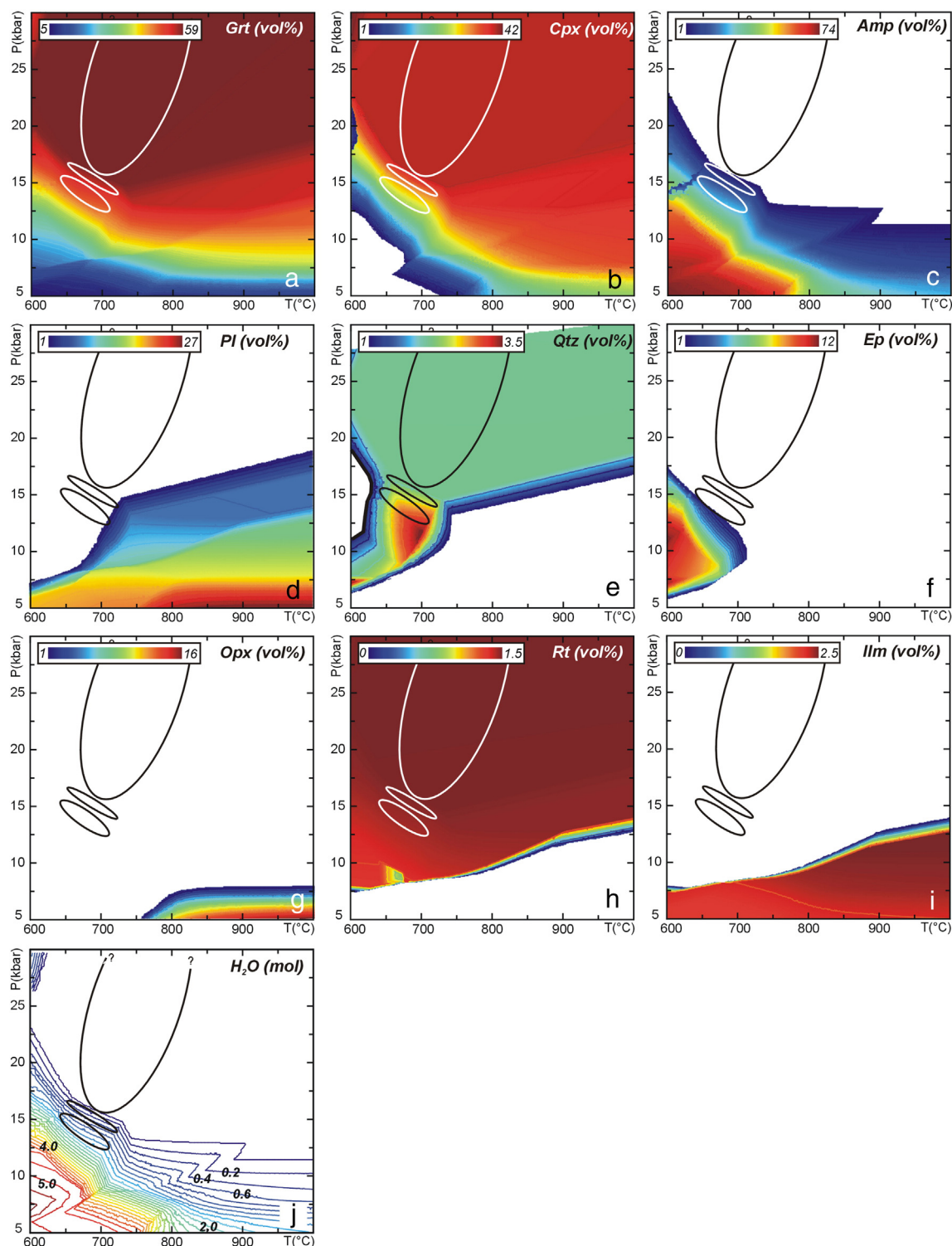


**Fig. 8.** (a–i) Modal variations (vol%) of the main mineral phases in sample 11-7c2 calculated for the P–T pseudosection of Fig. 7a. Colours from blue to red imply higher modal proportions as indicated in each legend. (j) Isomodes of water (mol). The ellipses are the same as in Fig. 7a.

compositional isopleths of garnet in this field ( $X_{\text{Mg}} = 0.35\text{--}0.50$ ,  $X_{\text{Ca}} = 0.19\text{--}0.24$ ) (Fig. SM3) do not perfectly fit with the observed  $\text{Grt}_2$  composition ( $X_{\text{Mg}} = 0.39\text{--}0.45$ ,  $X_{\text{Ca}} = 0.13\text{--}0.20$ ). This apparent discrepancy between modelled and measured garnet composition may be due to the fact that  $\text{Grt}_2$  was pervasively consumed at its rim during the following evolution and its original outermost composition has been lost.

Further P–T constraints for this assemblage are given by the  $\text{Pl}_{25} + \text{Spl} \pm \text{Crn}$  symplectite after kyanite, whose formation was initially triggered by the contemporaneous breakdown of kyanite and omphacite and growth of  $\text{Grt}_2$ , but that further reflects the attainment of equilibrium on a domainal scale. Considering the system CMAS ( $\text{CaO}\text{--}\text{MgO}\text{--}\text{Al}_2\text{O}_3\text{--}\text{SiO}_2$ ) and adjusting the activities of anorthite, grossular, diopside and spinel according to the measured plagioclase



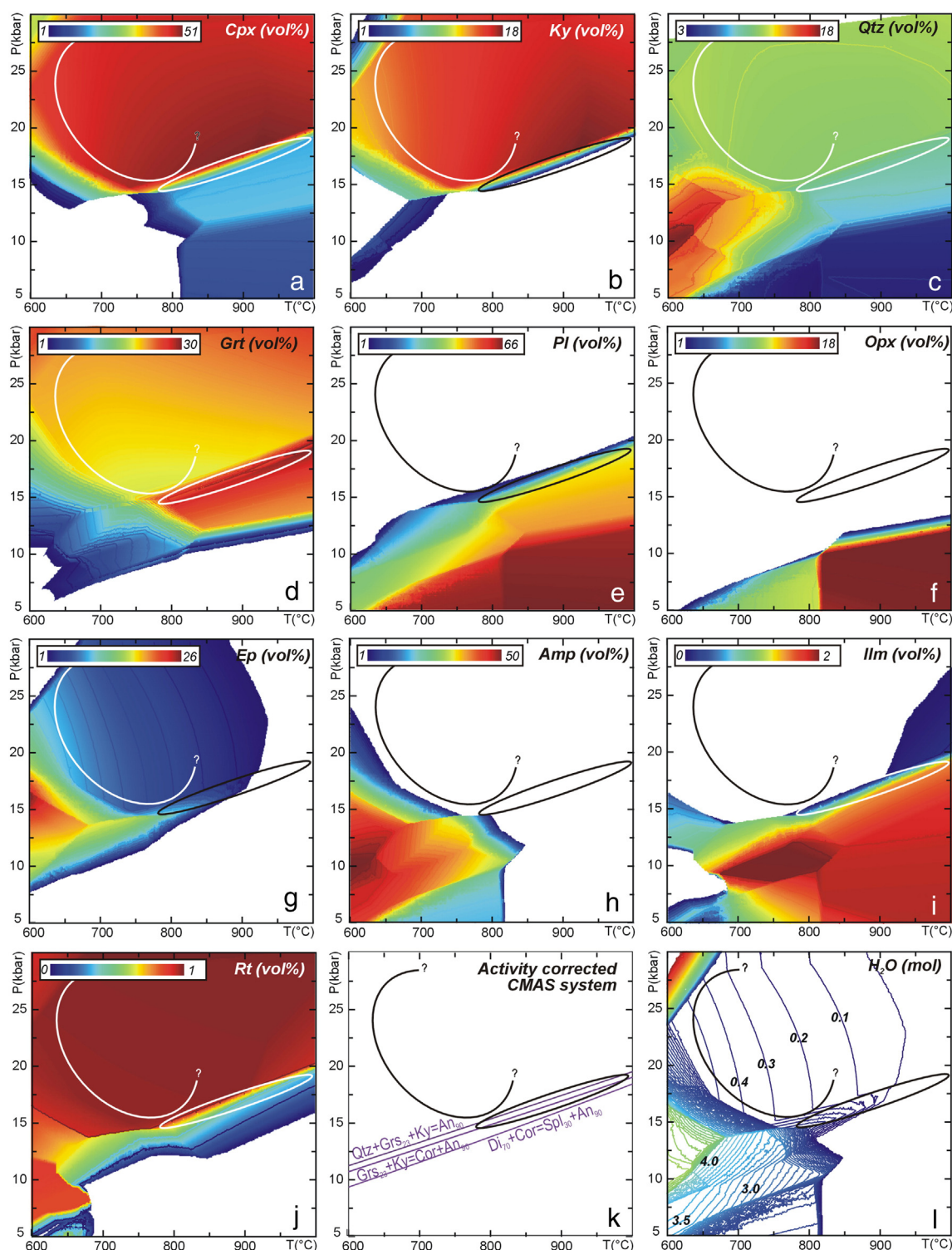


**Fig. 9.** (a–j) Modal variations (vol%) of the main mineral phases in sample 11-9c1 calculated for the P–T pseudosection of Fig. 7c. Colours from blue to red imply higher modal proportions as indicated in each legend. The ellipses are the same as in Fig. 7c. (k) Equilibria involving garnet, plagioclase, clinopyroxene, spinel and quartz calculated in the activity corrected CMAS system and constraining the formation of the strongly zoned pseudomorphs after kyanite. (l) Isomodes of water (mol).

(Pl<sub>2b</sub>), garnet (Grt<sub>2</sub>), clinopyroxene (Omp<sub>1</sub>) and spinel compositions, three equilibria can be considered:

- (i) Qtz + Grs<sub>23</sub> + Ky = An<sub>90</sub>
- (ii) Grs<sub>23</sub> + Ky = Cor + An<sub>90</sub>
- (iii) Di<sub>70</sub> + Cor = Spl<sub>30</sub> + An<sub>90</sub>

These three equilibria have a slightly positive slope in the P–T space (Fig. 9k) and constrain a narrow P interval of ca. 1.5 kbar, between 15 and 16.5 kbar at 800 °C. Although semi-quantitative (see also Godard and Mabit, 1998), this approach further suggests that assemblage 2 is the result of decompression from peak-P to ca. 15–18 kbar at T > 800 °C.

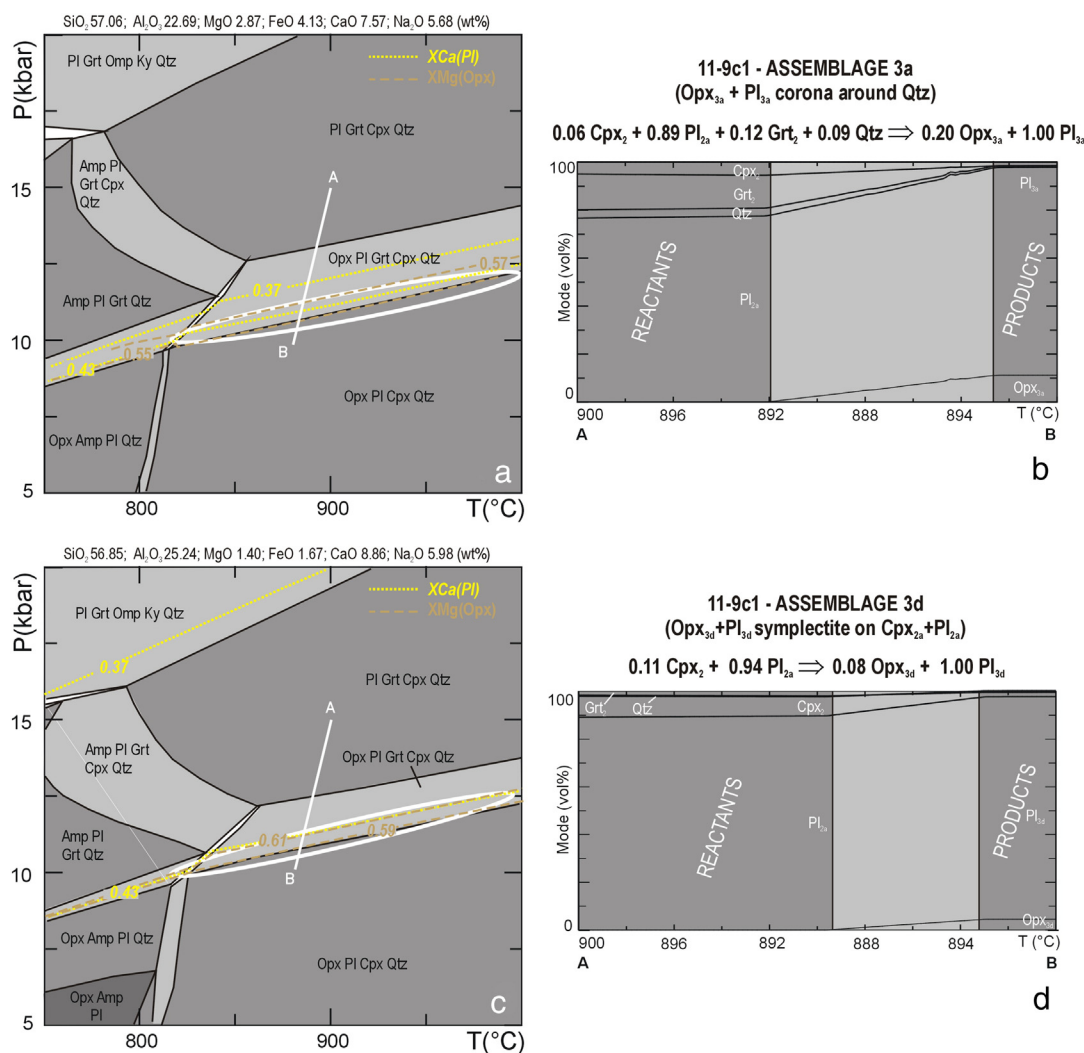


**Fig. 10.** Modelling of reaction microdomains. The P–T diagrams (a, c) and the modal evolutions (b, d), were modelled considering the composition of each reaction microdomain. P–T pseudosections and modal evolutions calculated for the microdomains 3a (Opx<sub>3a</sub> + Pl<sub>3a</sub> corona around Qtz) (a, b) and 3d (Opx<sub>3d</sub> + Pl<sub>3d</sub> symplectite in the matrix) (c, d) in sample 11-9c1, using the effective bulk compositions obtained from the balanced reactions (1) and (2), respectively. In all the pseudosections, the variance of the fields varies from two (i.e. 6 phases, white fields) to five (i.e. 3 phases, darker grey fields). The white ellipses constrain the P–T conditions of stages 3a and 3d respectively, as inferred from compositional isopleths of plagioclase ( $X_{\text{Ca}}$ ; yellow dotted lines), and orthopyroxene ( $X_{\text{Mg}}$ ; brown dashed lines). The entire set of isopleths and isomodes available at Figs. SM4–SM5. The proposed P–T paths (lines A–B) yield satisfactory modal evolutions for the reactions of interest (reactants → products).

### 6.3.2. Assemblage 3a (Opx<sub>3a</sub> ± Pl<sub>3a</sub> symplectitic corona around quartz)

This microstructure was modelled using the effective bulk composition obtained from the balanced reaction (1). The P–T pseudosection (Fig. 10a), calculated in the NCFMASH system, and the modelled modal evolution (Fig. 10b) show that reaction (1) occur at  $P < 13$  kbar and  $T > 800$  °C. Opx<sub>3a</sub> and Pl<sub>3a</sub> compositions (Opx:  $X_{\text{Mg}} = 0.55\text{--}0.57$ ; Pl:  $X_{\text{Ca}} = 0.37\text{--}0.43$ ) give tight constraints on  $P$  but poor information on  $T$ , constraining the growth of this microstructure at  $> 800$  °C, 10–12 kbar.

### 6.3.3. Assemblages 3b and 3c (inner and outer corona around garnet)

The inner and outer coronas surrounding garnet have been interpreted as formed simultaneously in response to gradients in the chemical potentials of the diffusing components between garnet and the matrix. Due to the difficulty in modelling the reactions involved in the double corona formation, the P–T conditions of its growth were not tightly constrained. However, the occurrence of orthopyroxene in the inner corona, suggest  $P < 12\text{--}13$  kbar and  $T > 800$  °C, compatible with the orthopyroxene stability field (Fig. 7c).

### 6.3.4. Assemblage 3d (Opx<sub>3d</sub> ± Pl<sub>3d</sub> symplectite)

The Opx<sub>3d</sub> + Pl<sub>3d</sub> symplectite overgrowing the Cpx<sub>2a</sub> + Pl<sub>2a</sub> symplectite was modelled using the effective bulk composition obtained from the balanced reaction (2). The P–T pseudosection (Fig. 10c) calculated in the NCFMASH system and the modelled modal evolution (Fig. 10d) show that this reaction occurred at  $P < 13$  kbar. Orthopyroxene ( $X_{\text{Mg}} = 0.59\text{--}0.61$ ) and plagioclase ( $X_{\text{Ca}} = 0.41\text{--}0.44$ ) compositions constrain the growth of this microstructure at  $> 800$  °C, 10–12 kbar.

## 7. Discussion

### 7.1. Potentials and limits of thermodynamic modelling applied to HT overprinted eclogites

The two rocks selected for this study have been chosen among tens of different samples because represent two extreme situations: (i) a well preserved eclogite-facies assemblage (sample 11-7c2) vs. (ii) a well-developed granulitic assemblage (sample 11-9c1); the two samples are therefore the best candidates for registering the HP/UHP vs. HT/UHT portions of the P–T evolution.

Sample 11-7c2 would be, in principle, the most suitable to constrain peak-P conditions; however, the results of the thermodynamic modelling show that its bulk composition is substantially not reactive at  $P > 16$  kbar. In other words, once that the anhydrous, high-variant, eclogite-facies assemblage Grt + Omp + Qtz + Rt was developed (Fig. 7a), nothing more happened along the prograde path: garnet and omphacite did not change their composition and the modal percentage of each phase remained constant in a very large P-T interval (Fig. 8). The advantage of such a situation is that sample 11-7c2, being not reactive during a long portion of its evolution, froze the evidence of its prograde history, thus allowing the reconstruction of the prograde portion of its P-T trajectory. However, in such a situation, the pseudosection approach fails in constraining the maximum pressures experienced by the eclogite. The only phase potentially useful to constrain peak-P conditions, especially if included within a rigid mineral such as garnet, would be quartz/coesite; however, the modal amount of quartz in this sample is very low ( $<1$  vol%) and a  $\text{SiO}_2$ -phase has not been observed included in garnet.

As concerning sample 11-9c1, the results of thermodynamic modelling show that at pressures  $> 15$  kbar the assemblage Grt + Omp + Ky + Qtz/Coe  $\pm$  Ep + Rt is stable over a large P-T interval (Fig. 7c), and that garnet (Grt<sub>1</sub>) is consumed and omphacite + kyanite are produced along any decompressional path from eclogite-facies toward HP granulite-facies (Fig. 9a,b,d). This means that the actually measured Grt<sub>1</sub> composition represents the composition of prograde garnet rather than that acquired at peak-P conditions. Furthermore, the possibility of finding coesite inclusions in garnet are vanished because the portion of garnet consumed during decompression is the same that potentially grew in the coesite stability field. Once again this situation hampered the precise determination of peak-P.

In contrast to sample 11-7c2, sample 11-9c1 is particularly reactive at HP granulite-facies conditions; this is due to the fact that sample 11-9c1 remained slightly  $\text{H}_2\text{O}$ -saturated during the early decompression evolution (see discussion below). However, the main reactions responsible for the breakdown of omphacite and kyanite and for the growth of Grt<sub>2</sub> are mainly P-dependent, thus providing good constraints on P but poor constraints on T. The texturally controlled thermodynamic microstructures allow to constrain precisely only the P-T conditions experienced in the low-P granulite-facies.

Therefore, the thermodynamic modelling approach has demonstrated to be a valuable method for reconstructing at least some portions of the P-T evolution of the Luotian dome eclogites. However, due to the HT overprinting and/or to poorly reactive bulk compositions, this method alone is not sufficient to reconstruct the whole P-T trajectory.

## 7.2. P-T evolution of the granulitized eclogites from the Luotian dome

Whether or not the NDZ as a whole underwent deep subduction and subsequent UHP metamorphism was a controversial issue for a long time (e.g. Zhang et al., 2009), essentially because diagnostic UHP phases such as coesite or micro-diamond were not found in the south-western part of the NDZ (i.e. the Luotian dome area). Liu et al. (2011a,b), basing on the discovery of a very small coesite inclusion within zircon and quartz pseudomorphs after coesite within garnet, suggested that the eclogites of the Luotian dome underwent UHP metamorphism and are therefore comparable to those from the north-eastern part of the NDZ. As a consequence, the whole NDZ would have behaved as a coherent unit during the Triassic subduction.

This detailed petrologic study using the pseudosection approach allowed to precisely constrain the following portions of the P-T trajectory experienced by the Luotian dome eclogites (Fig. 11):

- (i) A prograde increase in both P and T from ca. 650 °C, 12 kbar up to  $> 750$  °C,  $> 20$  kbar is recorded by assemblages 1 and 2 in sample

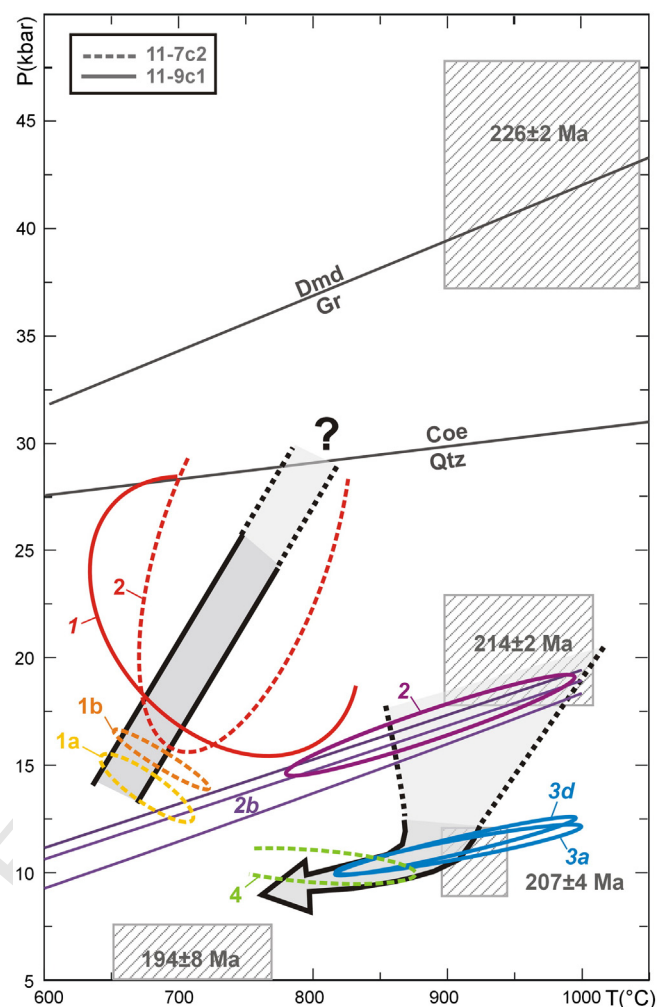


**Fig. 11.** Synthesis of the P-T constraints derived from the thermodynamic modelling approach applied to samples 11-7c2 (dashed ellipses) and 11-9c1 (continuous ellipses). Colours are the same as in Fig. 6. The dashed boxes with ages are the P-T estimates for the NDZ eclogites derived from Liu et al. (in press). The grey arrows are the portions of the P-T trajectory reconstructed in this study.

11-7c2. The first portion of this prograde trajectory is well constrained by garnet growth zoning and clinopyroxene composition. On the opposite, peak-P conditions are poorly constrained, being assemblage 2 nearly insensitive to pressure variations. Sample 11-9c1 roughly confirms these P-T conditions but does not help in better defining the peak-P conditions experienced by the Luotian dome eclogites, because eclogite-facies relics are poorly preserved, strongly re-equilibrated and decomposed or modified during the following HT evolution.

- (ii) The first important early-decompression event occurred at the transition from the eclogite- to the HP granulite-facies. In sample 11-9c1 this stage is documented by the breakdown of omphacite, kyanite and zoisite/epidote leading to the development of Cpx + Pl symplectites, of composite Spl + Pl  $\pm$  Crn symplectites, and of Pl + Mt aggregates, respectively. The formation of these symplectites is synchronous with the growth of a second garnet generation. This early decompression event is well constrained as concerning P (15–18 kbar), but poorly constrained as concerning T ( $> 800$  °C). Sample 11-9c1 is much more reactive at HP granulite-facies conditions than sample 11-7c2: this is due to different water availability in the two samples. The calculated  $\text{H}_2\text{O}$  isomodes for sample 11-7c2 (Fig. 8j) show that anhydrous conditions prevail during the early decompression evolution, whereas the system became  $\text{H}_2\text{O}$ -undersaturated at



$P < 15$  kbar, i.e. metamorphic reactions could not proceed until  $H_2O$ -saturated conditions were again reached or, alternatively,  $H_2O$  was introduced from outside (see Guiraud et al., 2001 for the interpretation of  $H_2O$ -saturated vs.  $H_2O$ -undersaturated conditions). In contrast, sample 11-9c1 remained  $H_2O$ -saturated during the early decompression evolution (i.e. the  $P$ - $T$  path intersects the  $H_2O$  isomode contours towards decreasing values, despite the overall  $H_2O$  content being extremely low; Fig. 9l) thus allowing the development of coronitic and symplectitic microstructures after omphacite and kyanite and the growth of Grt<sub>2</sub>.

- (iii) A later decompression event under lower- $P$  granulitic conditions characterized both the samples and is testified by the pervasive development of Opx-bearing coronitic, symplectitic and exsolution microstructures. The texturally controlled thermodynamic modelling applied to these microstructures tightly constrain this low- $P$  granulitic event at 800–900 °C, 10–12 kbar. The rare discontinuous Grt<sub>3</sub> rim locally overgrowing Grt<sub>2</sub> in sample 11-9c1 and including orthopyroxene and plagioclase, likely grew during, or immediately after, this stage. However, the limited occurrence of this microstructure in the studied sample hampers the precise constraint of the  $P$ - $T$  conditions of its growth.
- (iv) The pervasive growth of porphyroblastic amphibole in sample 11-9c1 and the formation of Amp + Pl coronae around garnet in sample 11-7c2 is related to a later hydration stage under upper amphibolite-facies conditions.

The overall clockwise  $P$ - $T$  trajectory (Fig. 11) deduced for the eclogites of the Luotian dome is therefore poorly constrained toward the extreme  $P$  and  $T$  conditions, and unambiguous evidence of the attainment of UHP and/or UHT conditions have not been found. However, although not sufficient to constrain the UHP peak  $P$ - $T$  conditions, the results of our study do not contradict the Liu et al. (2011a,b) conclusions. On the contrary, the prograde portion of the  $P$ - $T$  trajectory constrained here for the first time, is fully compatible with the extreme  $P$ - $T$  conditions proposed by Liu et al. (2011a,b) and Liu et al. (in press).

### 7.3. The North Dabie complex Zone: a “really hot and slow” UHP terrane

The resulting picture for the NDZ is that of a “really hot and slow” UHP terrane (McClelland and Lapen, 2013; see also Kylander-Clark et al., 2012), in contrast to the CDZ and SDZ terranes which are characterized by lower temperatures and different  $P$ - $T$  trajectories (“hot and slow” terranes of McClelland and Lapen, 2013). “Really hot and slow” UHP terranes such as the Greenland Caledonides (e.g. Gilotti et al., 2014), the Qaidam terrane of western China (Mattinson et al., 2006) or the Western Gneiss Region in Norway (e.g. Kylander-Clark et al., 2009) are thick (> 10 km) and exposed over large areas (> 20000 km<sup>2</sup>) (Kylander-Clark et al., 2012) and characterized by protracted UHP and exhumation histories, by slow exhumation rates and by a widespread anatexis, which may partially obliterate the direct evidence of UHP metamorphism.

This study demonstrated that, in such a case, the UHP metamorphism may be elusive and that the thermodynamic modelling approach may be not sufficient to unravel the whole  $P$ - $T$ -( $t$ ) evolution of “really hot and slow” UHP terranes. Different “unconventional” thermobarometric methods might be more suitable to decipher the HP/UHP history of these terranes (see also Hacker, 2006). It has been argued that U-Pb ages combined with trace element and textural characterization of zircon can successfully define the peak and the exhumation history of these UHP terranes (e.g. Gilotti et al., 2014): in this context the application of the recently calibrated Ti-in-zircon and Zr-in-rutile thermometers to the NDZ eclogites seem to be promising (Liu et al., in press). Rigid accessory phases such as zircon might often be the only direct witnesses of the UHP history: it is not incidental that, in most of the “really hot and

slow” UHP terranes, coesite and/or micro-diamonds have been found almost only as inclusions in zircons (e.g. Liu et al., 2007b; Xu et al., 2003).

## 8. Uncited reference

Torres-Roldan et al., 2000

## Acknowledgements

Study in the framework of the Cooperation agreement between the University of Turin (Italy) and the University of Science and Technology of China (School of Earth and Space Sciences - Hefei). Fieldwork and laboratory work supported by ex-60% funds of the University of Torino and by funds from the National Basic Research Program of China (2009CB825002) and the National Natural Science Foundation of China (41273036). We thank S. Ferrando for useful discussions and assistance in the field. The paper has been significantly improved thanks to the careful reviews by A. Proyer and Z. Tian. The Authors are very grateful to the Guest Editor, G. Godard, for his constructive suggestions and for having provided his mass-balance algorithm application.

## Appendix A. Supplementary data

Supplementary data to this article can be found online at <http://dx.doi.org/10.1016/j.lithos.2014.11.013>.

## References

- Adjerid, Z., Godard, G., Ouzegane, K., Kienast, J.-R., 2013. Multistage progressive evolution of rare osunilite-bearing assemblages preserved in ultrahigh-temperature granulites from In Ouzzal (Hoggar, Algeria). *Journal of Metamorphic Geology* 31, 505–524.
- Ames, L., Zhou, G., Xiong, B., 1996. Geochronology and isotopic character of high pressure metamorphism with implications for collision of the Sino-Korean and Yangtze cratons, central China. *Tectonics* 15, 472–489.
- Anderson, E.D., Moecher, D.P., 2007. Omphacite breakdown reactions and relation to eclogite exhumation rates. *Contributions to Mineralogy and Petrology* 154, 253–277.
- Bakun-Czubarow, N., 1992. Quartz pseudomorphs after coesite and quartz exsolutions in eclogitic omphacites of the Złote Mountains in the Sudetes (SW Poland). *Archiwum Mineralogiczne* 48, 3–25.
- Baldwin, J.A., Powell, R., Williams, M.L., Goncalves, P., 2007. Formation of eclogite, and reaction during exhumation to mid-crustal levels, Snowbird tectonic zone, western Canadian Shield. *Journal of Metamorphic Geology* 25, 953–974.
- Bryant, J.L., Ayers, J.C., Gao, S., Miller, C.F., Zhang, H., 2004. Geochemical, age, and isotopic constraints on the location of the Sino-Korean/Yangtze suture and evolution of the Northern Dabie Complex, east central China. *Geological Society of America Bulletin* 116, 698–717.
- Chavagnac, V., Jahn, B.M., 1996. Coesite-bearing eclogites from the Bixiling Complex, Dabie Mountains, China: Sm–Nd ages, geochemical characteristics and tectonic implications. *Chemical Geology* 133, 29–51.
- Chen, N.S., Sun, M., You, Z.D., Malpas, J., 1998. Well-preserved garnet growth zoning in granulite from the Dabie Mountains, central China. *Journal of Metamorphic Geology* 16, 213–222.
- Chen, Y., Ye, K., Liu, J.B., Sun, M., 2006. Multistage metamorphism of the Huangtuling granulite, Northern Dabie orogen, eastern China: implications for the tectonometamorphic evolution of subducted lower continental crust. *Journal of Metamorphic Geology* 24, 633–654.
- Cong, B., 1996. Ultrahigh-Pressure Metamorphic Rocks in the Dabieshan-Sulu Region of China. Science Press, Beijing (224 pp.).
- Connolly, J.A.D., 1990. Multivariable phase diagrams: an algorithm based on generalized thermodynamics. *American Journal of Science* 290, 666–718.
- Connolly, J.A.D., 2009. The geodynamic equation of state: what and how. *Geochemistry, Geophysics, Geosystems* 10, Q10014.
- Cossio, R., Borghi, A., Ruffini, R., 2002. Quantitative modal determination of geological samples based on X-ray multielemental map acquisition. *Microscope and Microanalysis* 8, 139–149.
- Cruciani, G., Franceschelli, M., Groppo, C., Brogioni, N., Vaselli, O., 2008. Formation of clinopyroxene + spinel and amphibole + spinel symplectites in coronitic gabbros from the Sierra de San Luis (Argentina): a key to post-magmatic evolution. *Journal of Metamorphic Geology* 26, 759–774.
- Cruciani, G., Franceschelli, M., Groppo, C., 2011.  $P$ - $T$  evolution of eclogite-facies metabasite from NE Sardinia, Italy: insights into the prograde evolution of Variscan eclogites. *Lithos* 121, 135–150.
- Cruciani, G., Franceschelli, M., Groppo, C., Spano, M.E., 2012. Metamorphic evolution of non-equilibrated granulitized eclogite from Punta de li Tulchi (Variscan Sardinia) determined through texturally controlled thermodynamic modeling. *Journal of Metamorphic Geology* 30, 667–685.

- Dale, J., Powell, R., White, R.W., Elmer, F.L., Holland, T.J.B., 2005. A thermodynamic model for Ca–Na clinopyroxenes in  $\text{Na}_2\text{O}$ – $\text{CaO}$ – $\text{FeO}$ – $\text{MgO}$ – $\text{Al}_2\text{O}_3$ – $\text{SiO}_2$ – $\text{H}_2\text{O}$ – $\text{O}$  for petrological calculations. *Journal of Metamorphic Geology* 23, 771–791.
- Dobrzynetskaia, L.F., Faryad, S.W., 2011. Frontiers of Ultrahigh-Pressure Metamorphism: View from Field and Laboratory. In: Dobrzynetskaia, L.F., Faryad, S.W., Wallis, S., Cuthbert, S. (Eds.), *Ultrahigh-Pressure Metamorphism. 25 Years After the Discovery of Coesite and Diamond*. Elsevier, pp. 1–39.
- Dobrzynetskaia, L.F., Schweinehage, R., Massonne, H.J., Green, H.W., 2002. Silica precipitates in omphacite from eclogite at Alpe Arami, Switzerland: evidence for deep subduction. *Journal of Metamorphic Geology* 20, 481–492.
- Elvelvold, S., Gilotti, J.A., 2000. Pressure–temperature evolution of retrogressed kyanite eclogites, Weinschenk Island, North–East Greenland Caledonides. *Lithos* 53, 127–147.
- Ernst, W.G., Tsujimori, T., Zhang, R., Liou, J.G., 2007. Permian–Triassic collision, subduction-zone metamorphism, and tectonic exhumation along the east Asian continental margin. *Annual Review of Earth and Planetary Sciences* 35, 73–110.
- Faure, M., Lin, W., Shu, L., Sun, Y., Scharer, U., 1999. Tectonics of the Dabieshan (eastern China) and possible exhumation mechanism of ultrahigh-pressure rocks. *Terra Nova* 11, 251–258.
- Faure, M., Lin, W., Scharer, U., Shu, L., Sun, Y., Arnaud, N., 2003. Continental subduction and exhumation of UHP rocks. Structural and geochronological insights from the Dabieshan (East China). *Lithos* 70, 213–241.
- Gayk, T., Kleinschrodt, R., Langosch, A., Seidel, E., 1995. Quartz exsolution in clinopyroxene of high-pressure granulite from the Munchberg Massif. *European Journal of Mineralogy* 7, 1217–1220.
- Giacomini, F., Bompalao, R.M., Ghezzi, C., 2005. Petrology and geochronology of metabasites with eclogite facies relics from NE Sardinia: constraints for the Palaeozoic evolution of Southern Europe. *Lithos* 82, 221–248.
- Gilotti, J.A., McClelland, W.C., Wooden, J.L., 2014. Zircon captures exhumation of an ultrahigh-pressure terrane, North-East Greenland Caledonides. *Gondwana Research* 25, 235–256.
- Godard, G., 2009. Two orogenic cycles in eclogite-facies gneisses of the Southern Armorican Massif (France). *European Journal of Mineralogy* 21, 1173–1190.
- Godard, G., Mabit, J.-L., 1998. Peraluminous sapphirine formed during retrogression of a kyanite-bearing eclogite from Pays de Léon, Armorican Massif. *Lithos* 43, 15–29.
- Green, E., Holland, T.J.B., Powell, R., 2007. An order-disorder model for omphacitic pyroxenes in the system jadeite-diopside-hedenbergite-acmite, with applications to eclogitic rocks. *American Mineralogist* 92, 1181–1189.
- Groppo, C., Lombardo, B., Castelli, D., Compagnoni, R., 2007a. Exhumation history of the UHPM Brossasco-Isasca Unit, Dora-Maira Massif, as inferred from a phengite-amphibole eclogite. *International Geology Review* 49, 142–168.
- Groppo, C., Lombardo, B., Rolfo, F., Pertusati, P.C., 2007b. Clockwise exhumation path of granulitized eclogites from the Ama Drime range (Eastern Himalayas). *Journal of Metamorphic Geology* 25, 51–75.
- Gu, X.F., 2012. Petrologic geochemistry and isotopic geochronology of the Luotian eclogites from the North Dabie complex zone, central China. (PhD thesis), University of Science and Technology of China (165 pp.).
- Guiraud, M., Powell, R., Rebay, G., 2001.  $\text{H}_2\text{O}$  in metamorphism and the preservation of metamorphic mineral assemblages. *Journal of Metamorphic Geology* 19, 445–454.
- Guy, B., 1984. Contribution to the theory of infiltration metasomatic zoning: the formation of sharp fronts: a geometrical model. *Bulletin de Mineralogie* 107, 93–105.
- Guy, B., 1993. Mathematical revision of Korzhinskii's theory of infiltration metasomatic zoning. *European Journal of Mineralogy* 5, 317–339.
- Hacker, B.R., 2006. Pressures and Temperatures of Ultrahigh-Pressure Metamorphism: Implications for UHP Tectonics and  $\text{H}_2\text{O}$  in Subducting Slabs. *International Geology Review* 48, 1053–1066.
- Hacker, B.R., Ratschbacher, L., Webb, L., McWilliams, M.O., Ireland, T., Calvert, A., Dong, S., Wenk, H.R., Chateigner, D., 2000. Exhumation of ultrahigh-pressure continental crust in east central China: Late Triassic–Early Jurassic tectonic unroofing. *Journal of Geophysical Research* 105, 13339–13364.
- Holland, T.J.B., Powell, R., 1998. An internally consistent thermodynamic dataset for phases of petrologic interest. *Journal of Metamorphic Geology* 16, 309–343.
- Jahn, B.M., Chen, B., 2007. Dabieshan UHP metamorphic terrane: Sr–Nd–Pb isotopic constraint to pre-metamorphic subduction polarity. *International Geology Review* 49, 14–29.
- Janák, M., Froitzheim, N., Lupták, B., Vrabec, M., Krogh Ravna, E.J., 2004. First evidence for ultrahigh-pressure metamorphism of eclogites in Pohorje, Slovenia: Tracing deep continental subduction in the Eastern Alps. *Tectonics* <http://dx.doi.org/10.1029/2004TC001641>.
- Katayama, I., Nakashima, S., 2003. Hydroxyl in clinopyroxene from the deep subducted crust: evidence for  $\text{H}_2\text{O}$  transport into the mantle. *American Mineralogist* 88, 229–234.
- Katayama, I., Parkinson, C.D., Okamoto, K., Nakajima, Y., Maruyama, S., 2000. Supersilicic clinopyroxene and silica exsolution in UHPM eclogite and pelitic gneiss from the Kokchetav massif, Kazakhstan. *American Mineralogist* 85, 1368–1374.
- Konzett, J., Frost, D.J., Proyer, A., Ulmer, P., 2008. The Ca–Eskola component in eclogitic clinopyroxene as a function of pressure, temperature and bulk composition: an experimental study to 15 GPa with possible implications for the formation of oriented  $\text{SiO}_2$ -inclusions in omphacite. *Contributions to Mineralogy and Petrology* 155, 215–228.
- Korzhinskii, D.S., 1970. *Theory of metasomatic zoning*. Clarendon Press, Oxford (162 pp.).
- Kylander-Clark, A.R.C., Hacker, B.R., Johnson, C.M., Beard, B.L., Mahlen, N.J., 2009. Slow subduction of a thick ultrahigh-pressure terrane. *Tectonics* <http://dx.doi.org/10.1029/2007TC002251>.
- Kylander-Clark, A.R.C., Hacker, B.R., Mattinson, C.G., 2012. Size and exhumation rate of ultrahigh-pressure terranes linked to orogenic stage. *Earth and Planetary Science Letters* 321–322, 115–120.
- Lang, H.M., Gilotti, J.A., 2007. Partial melting of metapelites at ultrahigh-pressure conditions, Greenland Caledonides. *Journal of Metamorphic Geology* 25, 129–147.
- Langone, A., Godard, G., Prosser, G., Caggianelli, A., Rottura, A., Tiepolo, M., 2009. P–T path of the Hercynian low-pressure rocks from the Mandatoriccio complex (Sila massif, Calabria, Italy): new insights for crustal scale evolution. *Journal of Metamorphic Geology* 28, 137–162.
- Larikova, T.L., Zaraisky, G.P., 2009. Experimental modelling of corona textures. *Journal of Metamorphic Geology* 28, 139–151.
- Li, S., Chen, Y., Cong, B., Zhang, Z., Zhang, R.Y., Liu, D., Hart, S.R., Ge, N., 1993. Collision of the North China and Yangtze Blocks and formation of coesite-bearing eclogites: timing and processes. *Chemical Geology* 109, 70–89.
- Li, X.P., Zheng, Y.F., Wu, Y.B., Chen, F.K., Gong, B., Li, Y.L., 2004. Low-T eclogite in the Dabie terrane of China: petrological and isotopic constraints on fluid activity and radiometric dating. *Contributions to Mineralogy and Petrology* 148, 443–470.
- Liati, A., Gebauer, D., Wysocki, R., 2002. U–Pb SHRIMP-dating of zircon domains from UHP garnet-rich mafic rocks and late pegmatoids in the Rhodope zone (N Greece): evidence for Early Cretaceous crystallization and Late Cretaceous metamorphism. *Chemical Geology* 184, 281–299.
- Liou, J.G., Ernst, W.G., Zhang, R.Y., Tsujimori, T., Jahn, B.M., 2009. Ultrahigh-pressure minerals and metamorphic terranes – the view from China. *Journal of Asian Earth Sciences* 35, 199–231.
- Liu, Y.-C., Li, S., Xu, S., Li, H., Jiang, L., Chen, G., Wu, W., Su, W., 2000. U–Pb zircon ages of the eclogite and tonalitic gneiss from the northern Dabie Mountains, China and multi-overgrowths of metamorphic zircons. *Geological Journal of China Universities* 6, 17–423 (in Chinese with English abstract).
- Liu, Y.-C., Xu, S., Li, S., Chen, G., Jiang, L., Zhou, C., Wu, W., 2001. Distribution and metamorphic P–T condition of the eclogites from the mafic-ultramafic belt in the northern part of the Dabie Mountains. *Acta Geologica Sinica* 75, 385–395 (in Chinese with English abstract).
- Liu, Y.-C., Li, S., Xu, S., Jahn, B.M., Zheng, Y.F., Zhang, Z., Jiang, L., Chen, G., Wu, W., 2005. Geochemistry and geochronology of eclogites from the northern Dabie Mountains, central China. *Journal of Asian Earth Sciences* 25, 431–443.
- Liu, D., Jian, P., Kroner, A., Xu, F., 2006. Dating of prograde metamorphic events deciphered from episodic zircon growth in rocks of Dabie–Sulu UHP complex, China. *Earth and Planetary Science Letters* 250, 650–666.
- Liu, Y.-C., Li, S.G., Gu, X.-F., Xu, S.T., Chen, G.B., 2007a. Ultrahigh-pressure eclogite transformed from mafic granulite in the Dabie orogen, east-central China. *Journal of Metamorphic Geology* 25, 975–989.
- Liu, Y.-C., Li, S.G., Xu, S.T., 2007b. Zircon SHRIMP U–Pb dating for gneisses in northern Dabie high T/P metamorphic zone, central China: implications for decoupling within subducted continental crust. *Lithos* 96, 170–185.
- Liu, Y.-C., Gu, X., Li, S., Hou, Z.H., Song, B., 2011a. Multistage metamorphic events in granulitized eclogites from the North Dabie complex zone, central China: evidence from zircon U–Pb age, trace element and mineral inclusion. *Lithos* 122, 107–121.
- Liu, Y.-C., Gu, X., Rolfo, F., Chen, Z., 2011b. Ultrahigh-pressure metamorphism and multistage exhumation of eclogite from the Luotian dome, North Dabie Complex Zone (central China): Evidence from mineral inclusions and decompression texture. *Journal of Asian Earth Sciences* 42, 607–617.
- Liu, Y.-C., Deng, L.-P., Gu, X.-F., Groppo, C., Rolfo, F., 2014. Application of Ti-in-zircon and Zr-in-rutile thermometers to constrain high-temperature metamorphism in eclogites from the Dabie orogen, central China. *Gondwana Research* (in press).
- Malaspina, N., Hermann, J., Scambelluri, M., Compagnoni, R., 2006. Multistage metasomatism in ultrahigh-pressure mafic rocks from the North Dabie Complex (China). *Lithos* 90, 19–42.
- Mattinson, C.G., Wooden, J.L., Liou, J.G., Bird, D.K., Wu, C.L., 2006. Age and duration of eclogite-facies metamorphism, North Qaidam HP/UHP terrane, Western China. *American Journal of Science* 306, 683–711.
- McClelland, W.C., Lapen, T.J., 2013. Linking time to the pressure-temperature path for ultrahigh-pressure rocks. *Elements* 9, 273–279.
- Möller, C., 1999. Sapphirine in SW Sweden: a record of Sveonorwegian (–Grenvillian) late-orogenic tectonic exhumation. *Journal of Metamorphic Geology* 17, 127–141.
- Morimoto, N., 1988. Nomenclature of Pyroxenes. *Mineralogy and Petrology* 39, 55–76.
- Nakamura, D., Hirajima, T., 2000. Granulite overprinting of ultrahigh-pressure metamorphic rocks, northern Su–Lu region, eastern China. *Journal of Petrology* 41, 563–582.
- Nakamura, D., Svojtka, M., Naumura, K., Hirajima, T., 2004. Very high-pressure (>4 GPa) eclogite associated with the Moldanubian Zone garnet peridotite (Nové Dvory, Czech Republic). *Journal of Metamorphic Geology* 22, 593–603.
- Newton, R.C., Charlu, T.V., Kleppa, O.J., 1980. Thermochemistry of the high structural state plagioclases. *Geochimica et Cosmochimica Acta* 44, 933–941.
- O'Brien, P.J., 1989. The petrology of retrograde eclogites of the Oberpfalz Forest, northeastern Bavaria, west Germany. *Tectonophysics* 157, 195–212.
- O'Brien, P., 1997. Garnet zoning and reaction textures in overprinted eclogites, Bohemian Massif, European Variscides: a record of their thermal history during exhumation. *Lithos* 41, 119–133.
- Okay, A.I., Xu, S., Sengor, A.M.C., 1989. Coesite from the Dabie Shan eclogites, central China. *European Journal of Mineralogy* 1, 595–598.
- Okrusch, M., Matthes, S., Klemd, R., O'Brien, P.J., Schmidt, K., 1991. Eclogites at the north-western margin of the Bohemian Massif: a review. *European Journal of Mineralogy* 3, 707–730.
- Page, F.Z., Essene, E.J., Mukasa, S.B., 2005. Quartz exsolution in clinopyroxene is not proof of ultrahigh pressures: evidence from eclogites from the Eastern Blue Ridge, Southern Appalachians USA. *American Mineralogist* 90, 1092–1099.
- Pouchou, J.L., Pichoir, F., 1988. Determination of mass absorption coefficients for soft X-rays by use of the electron microprobe. In: Newbury, D.E. (Ed.), *Microbeam Analysis*. San Francisco Press, San Francisco, CA, pp. 319–324.

- Powell, R., Holland, T.J.B., 1999. Relating formulations of the thermodynamics of mineral solid solutions: Activity modeling of pyroxenes, amphiboles, and micas. *American Mineralogist* 84, 1–14.
- Powell, R., Holland, T.J.B., 2008. On thermobarometry. *Journal of Metamorphic Geology* 26, 155–179.
- Proyer, A., Krenn, K., Hoinkes, G., 2009. Oriented precipitates of quartz and amphibole in clinopyroxene of metabasites from the Greek Rhodope: a product of open system precipitation during eclogite–granulite–amphibolite transition. *Journal of Metamorphic Geology* 27, 639–654.
- Proyer, A., Rolf, F., Castelli, D., Compagnoni, R., 2014. Diffusion-controlled metamorphic reaction textures in an ultrahigh-pressure impure calcite marble from Dabie Shan, China. *European Journal of Mineralogy* 26, 25–40.
- Rolf, F., Compagnoni, R., Wu, W., Xu, S., 2004. A coherent lithostratigraphic unit in the coesite–eclogite complex of Dabie Shan, China: geologic and petrologic evidence. *Lithos* 73, 71–94.
- Schmädicke, E., Müller, W.F., 2000. Unusual exsolution phenomena in omphacite and partial replacement of phengite by phlogopite + kyanite in an eclogite from the Erzgebirge. *Contributions to Mineralogy and Petrology* 139, 629–642.
- Smith, D.C., 1988. A review of the peculiar mineralogy of the “Norwegian coesite–eclogite province”, with crystal-chemical, petrological, geochemical and geodynamical notes and an extensive bibliography. In: Smith, D.C. (Ed.), *Eclogites and Eclogite-Facies Rocks*, pp. 1–206.
- Smith, D.C., 2006. The SHAND quaternary system for evaluating the supersilicic or subsilicic crystal-chemistry of eclogite minerals, and potential new UHPM pyroxene and garnet end-members. *Mineralogy and Petrology* 88, 87–122.
- Smyth, J.R., 1980. Cation vacancies and the crystal-chemistry of breakdown reactions in kimerlitic omphacites. *American Mineralogist* 65, 1185–1191.
- Song, S.G., Yang, J.S., Xu, Z.Q., Liou, J.G., Shi, R.D., 2003. Metamorphic evolution of the coesite-bearing ultrahigh-pressure terrane in the North Qaidam, Northern Tibet, NW China. *Journal of Metamorphic Geology* 21, 631–644.
- Tajčmanová, L., Konopásek, J., Schulmann, K., 2006. Thermal evolution of the orogenic lower crust during exhumation within a thickened Moldanubian root of the Variscan belt of Central Europe. *Journal of Metamorphic Geology* 24, 119–134.
- Terry, M.P., Robinson, P., Krogh Ravna, E.J., 2000. Kyanite eclogite thermobarometry and evidence for thrusting of UHP over HP metamorphic rocks, Nordøyane, Western Gneiss Region, Norway. *American Mineralogist* 85, 1637–1650.
- Tong, L., Jahn, B., Zheng, Y.-F., 2011. Diverse P–T paths of the northern Dabie complex in central China and its reworking in the early Cretaceous. *Journal of Asian Earth Sciences* 42, 633–640.
- Torres-Roldán, R.L., García-Casco, A., García-Sánchez, P.A., 2000. CSpace: an integrated workplace for the graphical and algebraic analysis of phase assemblages on 32-bit wintel platforms. *Computers & Geosciences* 26, 779–793.
- Tsai, C.H., Liou, J.G., 2000. Eclogite-facies relics and inferred ultrahigh-pressure metamorphism in the North Dabie Complex, central-eastern China. *American Mineralogist* 85, 1–8.
- Wang, X., Liou, J.G., Mao, H.K., 1989. Coesite-bearing eclogite from the Dabie Mountains in central China. *Geology* 17, 1085–1088.
- Wang, S., Li, S., An, S., Hou, Z., 2012. A granulite record of multistage metamorphism and REE behavior in the Dabie orogen: Constraints from zircon and rock-forming minerals. *Lithos* 136–139, 109–125.
- Wu, Y.B., Zheng, Y., Gao, S., Jiao, W., Liu, Y., 2008. Zircon U–Pb age and trace element evidence for Paleoproterozoic granulite-facies metamorphism and Archean crustal rocks in the Dabie Orogen. *Lithos* 101, 308–322.
- Xiao, Y., Hoefs, J., van den Kerkhof, A.M., Li, S.G., 2001. Geochemical constraints of the eclogite and granulite facies metamorphism as recognized in the Raobazhai complex from North Dabie Shan, China. *Journal of Metamorphic Geology* 19, 3–19.
- Xiao, Y., Hoefs, J., Kronz, A., 2005. Compositionally zoned Cl-rich amphiboles from North Dabie Shan, China: monitor of high-pressure metamorphic fluid/rock interaction processes. *Lithos* 81, 279–295.
- Xie, Z., Zheng, Y.F., Zhao, Z.F., Wu, Y.B., Wang, Z., Chen, J., Liu, X., Wu, F.Y., 2006. Mineral isotope evidence for the contemporaneous process of Mesozoic granite emplacement and gneiss metamorphism in the Dabie orogen. *Chemical Geology* 231, 214–235.
- Xie, Z., Chen, J., Cui, Y., 2010. Episodic growth of zircon in UHP orthogneisses from the North Dabie Terrane of east-central China: implications for crustal architecture of a collisional orogen. *Journal of Metamorphic Geology* 28, 979–995.
- Xu, S., Okay, A.I., Ji, S., Sengör, A.M.C., Su, W., Liu, Y.-C., Jiang, L., 1992. Diamond from the Dabie Shan metamorphic rocks and its implication for tectonic setting. *Science* 256, 80–82.
- Xu, S., Liu, Y.-C., Su, W., Wang, R., Jiang, L., Wu, W., 2000. Discovery of the eclogite and its petrography in the Northern Dabie Mountain. *Chinese Science Bulletin* 45, 273–278.
- Xu, S., Liu, Y.-C., Chen, G., Compagnoni, R., Rolf, M., He, M., Liu, H., 2003. New findings of microdiamonds in eclogites from Dabie–Sulu region in central-eastern China. *Chinese Science Bulletin* 48, 988–994.
- Xu, S., Liu, Y.-C., Chen, G., Ji, S., Ni, P., Xiao, W., 2005. Microdiamonds, their classification and tectonic implications for the host eclogites from the Dabie and Su–Lu regions in central eastern China. *Mineralogical Magazine* 69, 509–520.
- Zhang, R.Y., Liou, J.G., 1998. Ultrahigh-pressure metamorphism of the Sulu terrane, eastern China: a prospective view. *Continental Dynamics* 3, 32–53.
- Zhang, R.Y., Liou, J.G., Tsai, C.H., 1996. Petrogenesis of a high-temperature metamorphic terrane: a new tectonic interpretation for the north Dabieshan, central China. *Journal of Metamorphic Geology* 14, 319–333.
- Zhang, L.F., Ellis, D.J., Jiang, W.B., 2002. Ultrahigh-pressure metamorphism in western Tianshan, China: Part I. Evidence from inclusions of coesite pseudomorphs in garnet and from quartz exsolution lamellae in omphacite in eclogites. *American Mineralogist* 87, 853–860.
- Zhang, L.F., Ellis, D., Williams, S., Jiang, W.B., 2003. Ultrahigh-pressure metamorphism in eclogites from the western Tianshan, China - Reply. *American Mineralogist* 88, 1157–1160.
- Zhang, L., Song, S., Liou, J.G., Ai, Y., Li, X., 2005. Relict coesite exsolution in omphacite from Western Tianshan eclogites, China. *American Mineralogist* 90, 181–186.
- Zhang, Z., Shen, K., Liou, J., Zhao, X., 2007. Fluid inclusions associated with exsolved quartz needles in omphacite of UHP eclogites, Chinese Continental Scientific Drilling main drill-hole. *International Geology Review* 49, 479–486.
- Zhang, R.Y., Liou, J.G., Ernst, W.G., 2009. The Dabie–Sulu continental collision zone: a comprehensive review. *Gondwana Research* 16, 1–26.
- Zhao, Z.F., Zheng, Y.F., Wei, C.S., Wu, Y.B., 2004. Zircon isotope evidence for recycling of subducted continental crust in post-collisional granitoids from the Dabie terrane in China. *Geophysical Research Letters* 31, L22602.
- Zhao, Z.F., Zheng, Y.F., Wei, C.S., Wu, Y.B., 2007. Post-collisional granitoids from the Dabie orogen in China: zircon U–Pb age, element and C–O isotope evidence for recycling of subducted continental crust. *Lithos* 93, 248–272.
- Zhao, Z.F., Zheng, Y.F., Wei, C.S., Chen, F.K., Liu, X., Wu, Y.B., 2008. Zircon U–Pb ages, Hf and O isotopes constrain the crustal architecture of the ultrahigh-pressure Dabie orogen in China. *Chemical Geology* 253, 222–242.
- Zhao, S., Nee, P., Green, H.W., Dobrzynetskaia, L.F., 2011. Ca–Eskola component in clinopyroxene: Experimental studies at high pressures and high temperatures in multianvil apparatus. *Earth and Planetary Science Letters* 307, 517–524.
- Zhu, Y., Ogasawara, Y., 2002. Phlogopite and coesite exsolution from super-silicic clinopyroxene. *International Geology Review* 44, 831–836.